PHOTOLUMINESCENCE SPECTROSCOPY OF ZINC GERMANIUM DIPHOSPHIDE ($ZnGeP_2$)

THESIS

Jack E. McCrae., Jr., Captain, USAF

AFIT/GAP/ENP/93S-01

AFIT/GAP/ENP/93S-01

PHOTOLUMINESCENCE SPECTROSCOPY OF ZINC GERMANIUM DIPHOSPHIDE ($ZnGeP_2$)

THESIS

Presented to the Faculty of the School of Engineering

of the Air Force Institute of Technology

Air University

in Partial Fulfillment of the

Requirements for the Degree of

Master of Science in Engineering Physics

Jack E. McCrae., Jr.

Captain, USAF

September 1993

Approved for public release; distribution unlimited

Acknowledgments

This study has proven to be both interesting and challenging. I would like to thank my advisors, Dr R. L. Hengehold, Dr Y. K. Yeo, and Maj P. H. Ostdiek for both steering me to this project and seeing me through it. I would also like to thank Dr M. C. Ohmer, of the Wright Laboratory's Materials Directorate for providing the samples used and inviting AFIT to join in the exploration of this material's properties. Additionally, I would like to thank Mr Greg Smith for his assistance in the laboratory and his help in obtaining needed equipment. Finally, I would like to thank my wife, Kimberley, for her support, encouragement, and editorial assistance.

Table of Contents

List of Figures

List of Tables

Abstract

Zinc germanium diphosphide ($ZnGeP_2$) is a chalcopyrite semiconductor with strong nonlinear optical properties and potential application to Air Force interests. The characteristics of this material have been studied using photoluminescence (PL) spectroscopy. The PL spectrum is dominated by transitions from the conduction band to a deep acceptor level, and features in the spectrum suggest that more than one transition is being observed. The PL is partially polarized, and the degree of polarization appears to differ for each feature in the spectrum. The relative PL intensity of these features are seen to depend upon the wavelength of the excitation source in a fashion which suggests that the observed transitions may originate from three separate conduction bands. These experimentally observed results are found to agree qualitatively with the published band structure of $ZnGeP_2$.

I. Overview

$ZnGeP_2$ is a semiconductor with strong nonlinear optical properties suitable for use in novel laser devices, thereby motivating Air Force interest. The goal of this research is to build a better understanding of $ZnGeP_2$ through the use of PL spectroscopy. The basics of semiconductor physics are discussed to develop the idea of the electronic band structure of materials, and to explain the origin of luminescence in opto-electronic materials. These concepts are applied to $ZnGeP_2$ in particular, and the features of this material are discussed. Previous work in the growth and characterization of $ZnGeP_2$ is reviewed.

The experimental approach is discussed next. The equipment used and the experimental layout are described in detail. The operation of the equipment is outlined and the PL spectra measured are displayed. The effects of differing polarizations, excitation energies, laser powers, and material samples are investigated. The PL spectra are seen to be strongly polarized overall, with features seen in each spectrum showing varying degrees of polarization. The relative magnitude of these spectral features is seen to be strongly dependent upon the excitation wavelength. These results are related back to the band structure of this material, showing good agreement with published band parameters. Possible sources of experimental error are examined. Conclusions are drawn as to the nature of the observed PL spectra and the reliability of these determinations. It is further concluded that the quality of one of the samples examined is higher than any used in previous studies. A number of recommendations are made for further study and for improving the experimental layout. An explanation of experimental artifacts seen on cathodoluminescence data is presented in an appendix, as is the calibration data for the spectrometer.

II. Background

$ZnGeP_2$ shows promise as the key element in producing a tunable laser device, called an Optical Parametric Oscillator (OPO) (Shay and Wernick, 1975:152; Budni et al,

1992:380). An OPO made with $ZnGeP_2$ could operate at high power with continuous tunability from 2 to 6 μm. This wavelength range is particularly interesting for several Air Force applications since it is considered eye-safe and it covers a large atmospheric transmission window. This is the main reason for Air Force interest in this material. $ZnGeP_2$ has been successfully used for frequency up-conversion at a variety of wavelengths in the infrared (Andreev et al., 1992:1035; Vodopyanov et al., 1991:322). The utilization of $ZnGeP_2$ has been obstructed by strong absorption in the near-infrared exhibited by materials grown in the past. This absorption would restrict the tuning range, output power, and pump wavelength of an OPO utilizing $ZnGeP_2$. It is believed that this absorption is due to imperfections in the crystal (Hobgood et al., 1992:4030). Recently, advances in growth and processing techniques have mitigated this problem somewhat (Hobgood et al., 1992:4030), and it is hoped that a better understanding of the material's properties can show the way to producing better material for devices.

III. Theory

3.1 Quantum Mechanics

The allowed energy states of an electron in a crystal may be computed using the time-independent Schrödinger equation

$$-\frac{\hbar^2}{2m}\nabla^2\psi + V\psi = E\psi \ ,$$

where ψ is the electron wavefunction, m is the electron mass, V is the potential due to every atom in the crystal, and E is the electron energy. In the case of a perfect, infinite crystal, V will be periodic. In the case of a periodic potential, Bloch's theorem states that the allowed wavefunctions, called Bloch functions, can be written as the product between a phase term (which has the form of a plane wave) and another function (u) which has the same periodicity as the potential. (McKelvey, 1966:211) That is

$$\psi_{\bar{k}}(\bar{r}) = e^{i\bar{k}\cdot\bar{r}}u_{\bar{k}}(\bar{r}) \ .$$

To keep ψ finite everywhere, $\bar{k}$, the wavevector, must be real, and for each real wavevector Schödinger's equation can be solved (at least in principle) to give a real E, but the converse is not true. There are ranges of values of E for which no real $\bar{k}$ can be found. Allowed values of energy are separated by gaps called forbidden bands or energy gaps. These energy gaps occur at locations of $\bar{k}$ for which the electron wave function will undergo Bragg reflection.

3.2 Band Structure

For simplicity, the one dimensional case may be examined more closely; this is essentially equivalent to considering a particular direction in a real crystal. The Bloch function can be written one dimensionally as

$$\psi_k(x) = e^{ikx} u_k(x) \ .$$

For a crystal of periodicity a, factors of $e^{i\frac{\pi}{a}x}$ may be moved freely between the phase term and u_k term since factors like this have both the periodicity of the crystal and the form of a plane wave. Thus, the selection of a value for k is somewhat ambiguous since k is only uniquely defined within a $2\pi/a$ range. Two different approaches are taken to deal with this: the expanded zone representation and the reduced zone representation. In the expanded zone representation, successively higher values of k are assigned to increasing values of E. This relates nicely to the relationship between energy and wavevector for a free or nearly free particle. In the reduced zone representation all values of k are kept between $-\pi/a$ and $+\pi/a$. This representation gives the same value of k to wavefunctions whose relationship is the same within each crystal period. Wavefunctions like this might be expected to interact strongly since their interaction is summed constructively in each successive crystal period. Indeed, this is the case, as will be discussed below. A hypothetical plot of E vs. k, illustrating some of these points, is shown as figure 1. The reduced zone representation is also apparent in figure 1 between $-\pi$ and π on the horizontal axis. The darkened lines can be folded back along the vertical lines (where $ka = n\pi$, n being any integer) to overlay the light lines, illustrating the

equivalence of the reduced and expanded zone representations. The quantity, $\hbar k$, has units of momentum, and is also known as the crystal momentum, or quasi-momentum. The requirement that transitions between bands conserve k can thus be stated as a conservation of momentum condition.

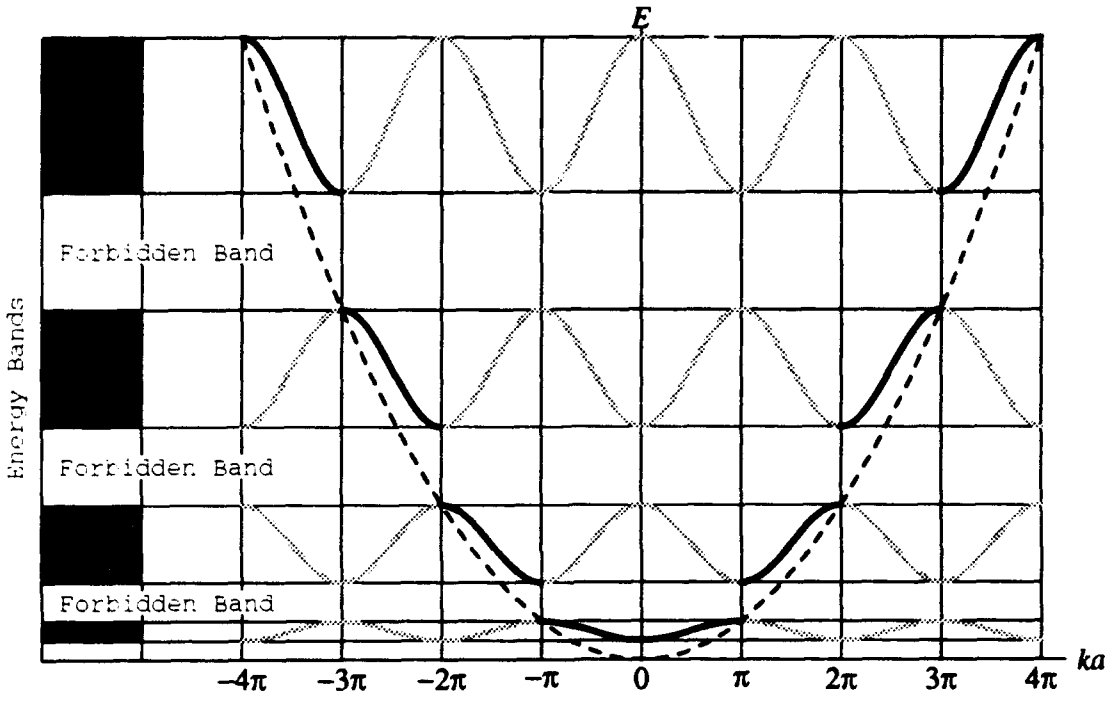

Figure 1. Expanded zone representation of energy band diagram. The darkened lines show the convention for choosing k in the expanded zone representation. Allowed energy bands are darkly shaded on the left. The dotted line shows the relationship between E and k for a free particle; that is $E = \hbar^2 k^2 / 2m$. (Liboff, 1980:276)

3.2 Material Properties

Materials can be either conductors, insulators or semiconductors, depending upon the occupancy of the allowed bands. The electrons in a material will try to achieve the lowest energy state, thus the bands described above will be filled from the lowest to the highest as electrons are added (conceptually) to a material. If the highest occupied band

in a material is partially full, the material can be expected to be a conductor since electrons can acquire a small amount of energy from an applied electric field to achieve a slightly higher energy state and move across the crystal – this is essentially the case for metals. If, however, the highest occupied band is filled, and the next band is empty, then an electron must jump all the way to the next band in order to increase in energy. If the next band is too far away for the electron to have a reasonable chance of undergoing a transition up, and if the temperature is low enough that an electron will not be likely to have this much thermal energy, then the material will behave as an insulator. In between these two extremes, we have semiconductors. Semiconductors are materials which may have a small number of electrons in their highest occupied band (the conduction band), or a small number of unfilled states in the next lower band (the valence band) due to either the thermodynamic occupancy of states or some specific tailoring. The energy separation between the conduction and valence bands is called the bandgap. If a band is nearly full, it is easier to study the few empty states, now called holes, than the many full ones; for all practical purposes the holes behave as positive charge carriers. In the discussion above, 'small number' is a relative term, counted with respect to the number of states in a band. In silicon or diamond, for instance, there are 4 states available in each the conduction and the valence band for every atom in the crystal. The presence of one electron in the conduction band per million atoms is more than enough to cause measurable conductance. There are several ways to add extra electrons or holes in the semiconductor energy bands. If a small percentage of the atoms in a semiconductor are replaced by atoms having more electrons in their valence band than the atoms they replace, then extra electrons are available to occupy states in the conduction band. Elements added in this fashion are called dopants, and in the case where they can provide additional electrons to the crystal, they are called electron donors, or just donors. Before the extra electrons added by the donor can move freely about the crystal, they must overcome the coulomb attraction of the dopant atom. Typically this ionization energy is a few hundredths of an

electron volt of energy for a well selected dopant, an amount that is readily available thermodynamically at room temperature. Conversely, if the dopant contains fewer valence electrons than the atom it replaces, it will be able to accept electrons from the valence band, leaving a hole behind in the valence band, which will be free to move around the crystal; it is thus called an acceptor. Donor and acceptor levels can be thought of as lying within the bandgap, separated from their respective energy bands by their ionization energies. Electrons may also be added to the conduction band by promoting them from the valence band. In the case of a semiconductor with a small bandgap, this might be likely to happen thermally at reasonable temperatures, otherwise an external excitation source is required to provide the energy to bridge the bandgap and create electron-hole pairs. A sufficiently energetic photon, for instance, is capable of providing the energy to promote an electron from the valence band to the conduction band. The reverse process is also possible, thereby creating a photon.

3.4 Luminescence

There are many mechanisms by which semiconductor material can emit light. In short, when an electron moves from a high to a low energy state a photon might be emitted. Figure 2 illustrates several of these possibilities. The wavelength of the emitted photon can be used to identify the mechanism whereby it was created, making luminescence spectroscopy an excellent diagnostic tool for probing impurity energy levels and the band structure of materials. The transitions outlined in figure 2 are grouped into three classes: (1) interband transitions, (2) transitions involving impurities or defects and (3) hot carrier intraband transitions. The first category is further broken down into (a) near-band-edge band to band transition and (b) hot carrier band to band transition. The second category consists of (a) conduction band to acceptor level, (b) donor level to valence band, (c) donor to acceptor level and (d) deep level transitions. Any of these illustrated transitions could result in the emission of a photon; whether this is likely or not depends upon both the transition mechanism and the material. Many other

considerations serve to further complicate this already complex topic. An electron and a hole can orbit each other about their common center of mass; this hydrogen-atom-like system is called an exciton. Excitons can only exist for a meaningful length of time at very low temperatures. Since the electron and the hole attract each other, an exciton has less potential energy than a free pair of charge carriers. Thus when an exciton recombines, any photon which is emitted has slightly less energy than the bandgap. Since this photon doesn't have quite enough energy to re-excite an electron from the valence band into the conduction band, it has a much better chance to escape from the crystal than photons created by transitions at or above the bandgap. Luminescence caused by transitions from the conduction band to an acceptor level is often called impurity luminescence; it is still be called impurity luminescence even when the acceptor level is created by a crystal defect, rather than an actual impurity.

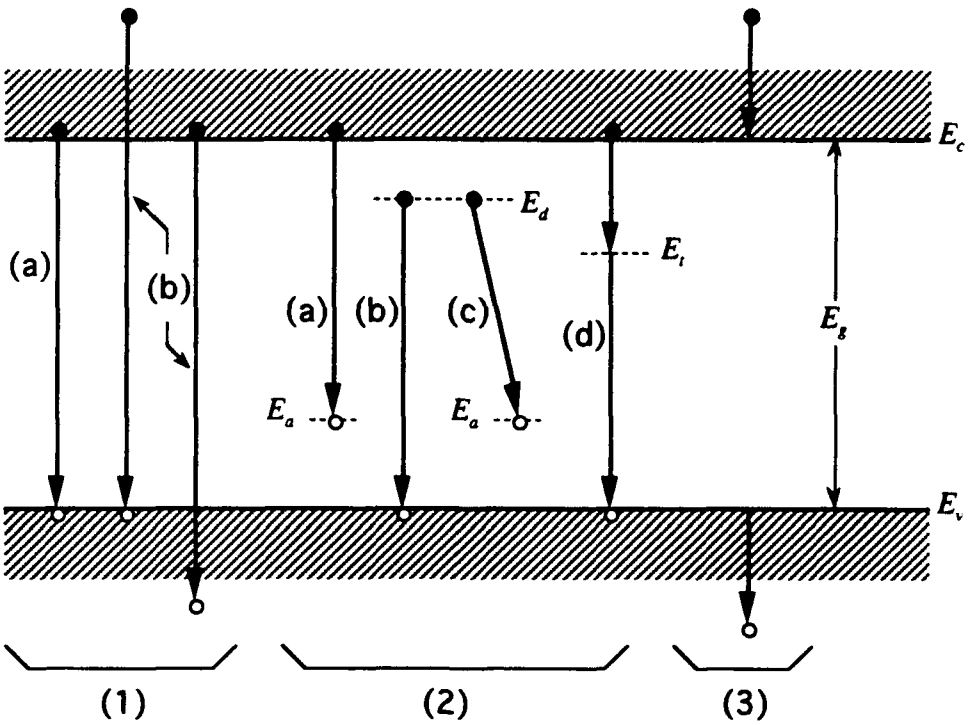

Figure 2. Basic transitions in a semiconductor. E_g is the bandgap, E_v marks the top of the valence band, E_c marks the bottom of the conduction

band, E_a is an acceptor level, E_d is a donor level, and E_t is a trap level. (Sze, 1981:684)

If we return to the reduced zone representation of the band structure, another distinction becomes apparent. Semiconductors may be either direct gap, or indirect gap materials, depending upon whether or not the maximum of the valence band and the minimum of the conduction band occur for the same value of k. Figure 3 compares these two possibilities, and contrasts their light emitting mechanisms.

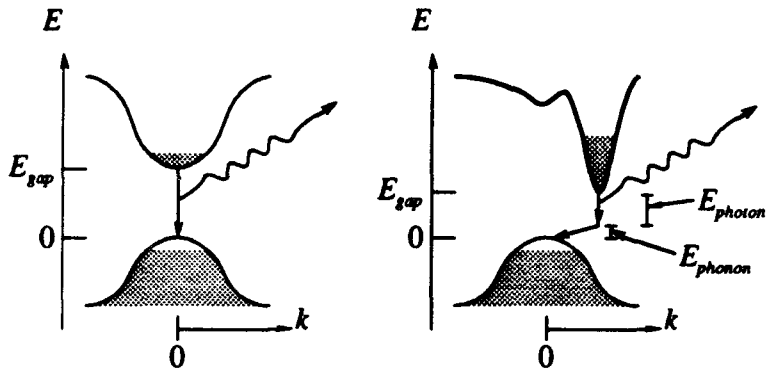

Figure 3. Direct vs. indirect bandgap transitions. (a) Electron and hole recombine and a photon is emitted. (b) Electron and hole recombine, emitting a photon and a phonon. (Pankove, 1971:124,126)

Because electrons will tend to equilibrate to the lowest energy state available, the top of the valence band will collect holes, as electrons move down into available lower energy states. For the same reason, the bottom of the conduction band will collect electrons. In a material with a direct gap, the *k* values of these distributions will overlap, and photons can be emitted as carriers recombine directly. In a material with an indirect gap however, the story is not so simple. Since a transition from the conduction band to the valence band involving only the emission of a photon will not conserve crystal momentum, it is highly unlikely. In order for an electron to have a transition directly from the conduction to the valence band, the electron may emit both a phonon and a photon, thus allowing both momentum and energy to be conserved.

3.5 Photoluminescence and Cathodoluminescence Spectroscopy

Two useful techniques for probing the impurity levels in semiconductors are photoluminescence (PL) and cathodoluminescence (CL) spectroscopy. The essence of PL ectroscopy is relatively simple: a light source, typically a laser, is shined upon a sample of the material under consideration, photons emitted by the sample are analyzed with a spectrometer. The laser provides the energy required to excite electrons from the valence to the conduction band, thus producing electron-hole pairs, and when these electrons and holes recombine a photon may be emitted. It is, therefore, important that the laser's wavelength be short enough to excite electrons from the valence band to the conduction band. The laser's wavelength and power can both be varied to help extract additional information from the PL spectrum.

In the case of CL spectroscopy, an electron beam provides the energy to produce electron-hole pairs, mainly through impact ionization. An electron gun is used to generate and focus a stream of electrons. The total beam current, the direction of the beam, the focus of the beam, and the energy each electron carries may be varied by the gun. The accelerating voltage used by the gun determines how much energy each electron will receive, and is typically several orders of magnitude more energy than needed to excite an electron from the valence to the conduction band. Thus CL is a particularly useful technique for examining higher lying conduction bands and materials with wide bandgaps when lasers with sufficient photon energy are not readily available.

IV. The Properties of $ZnGeP_2$

4.1 Crystal Structure of $ZnGeP_2$

$ZnGeP_2$ is a chalcopyrite semiconductor, meaning its crystal structure is the same as the mineral chalcopyrite ($CuFeS_2$). This structure is shown in figure 4 , along with the zincblende structure, to which it is closely related. The chalcopyrite structure is seen to be made of two stacked zincblende structures, in which the cation (zinc) locations in

zincblende have been filled by a particular arrangement of alternating zinc and germanium atoms in $ZnGeP_2$. In the case of $ZnGeP_2$ the structure is also slightly compacted along the c axis, compared to the relative spacing seen in zincblende.

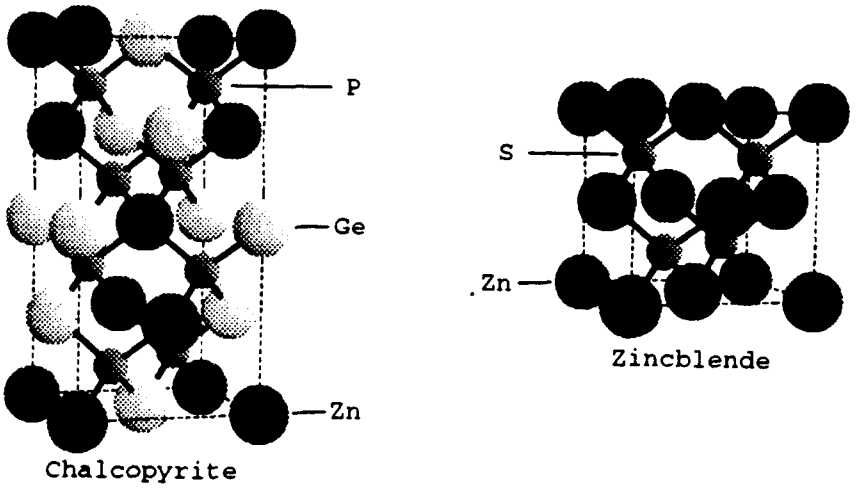

Figure 4. Chalcopyrite and zincblende crystal structures compared. (Shay and Wernick, 1973:6)

4.2 Band Structure of $ZnGeP_2$

The well ordered fashion in which Zinc and Germanium fill the lattice has a strong effect on the crystal's properties. Since Zinc and Germanium have differing bond lengths to Phosphorus in this material, the crystal symmetry is slightly distorted. This enhances the magnitude of the material's anisotropic and nonlinear optical properties. A primitive cell four times as large as that of the zincblende structure is needed to accommodate the chalcopyrite structure, again due to the regular placement of Zn and Ge atoms in the lattice. The four-fold growth in the volume of the unit cell in real space then results in a four-fold decrease in the volume of the Brillouin zone in reciprocal lattice space. Figure 5 shows the Brillouin zone of the chalcopyrite structure within the Brillouin zone of the zincblende structure. The bands of the otherwise analogous GaP

can be folded in to generate an approximated band structure of $ZnGeP_2$ as shown in figure 6.

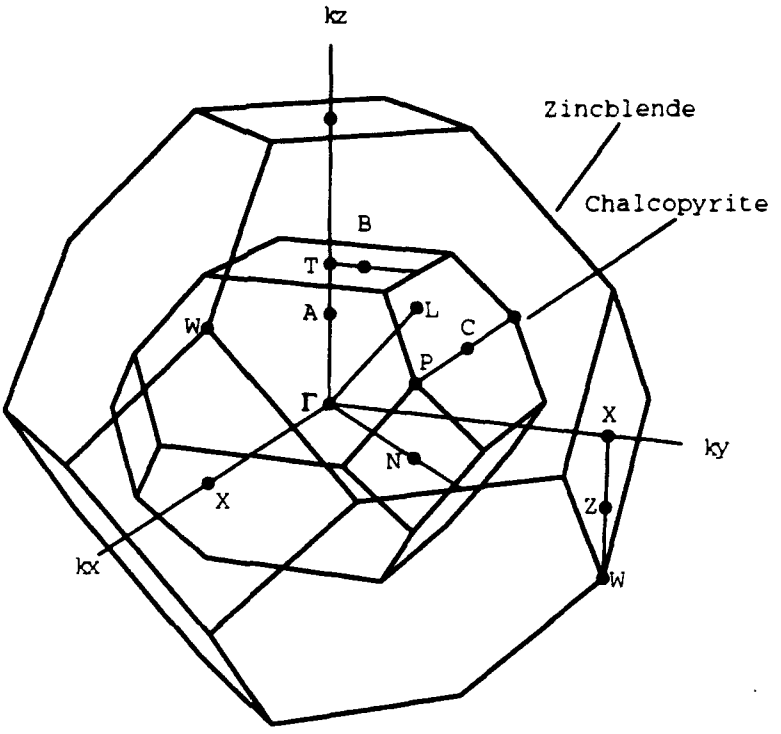

Figure 5. Comparison of the Brillouin zones of zincblende and chalcopyrite structures. (Shileika, 1973:731)

This folding causes the indirect bandgap seen in GaP to appear as a direct bandgap in $ZnGeP_2$. This bandgap is called pseudo-direct because transitions at this critical point are only allowed to the extent that Zn and Ge behave differently within the lattice (Shay and Wernick, 1975:80). Because the effects of Zn and Ge on the lattice are not greatly different, the pseudo-direct transition should be weak. If the cations (Zn and Ge in this case) were indistinguishable to an electron traveling through the crystal, then the folding of the bands would be in principle only; the bandgap would appear to be indirect to any optical or electrical experiments which might be carried out. The band structure

illustrated in figure 6 ignores the effects of spin-orbit interactions. If this effect is taken into account, the bands will be seen to split into sub-bands as shown in figure 7.

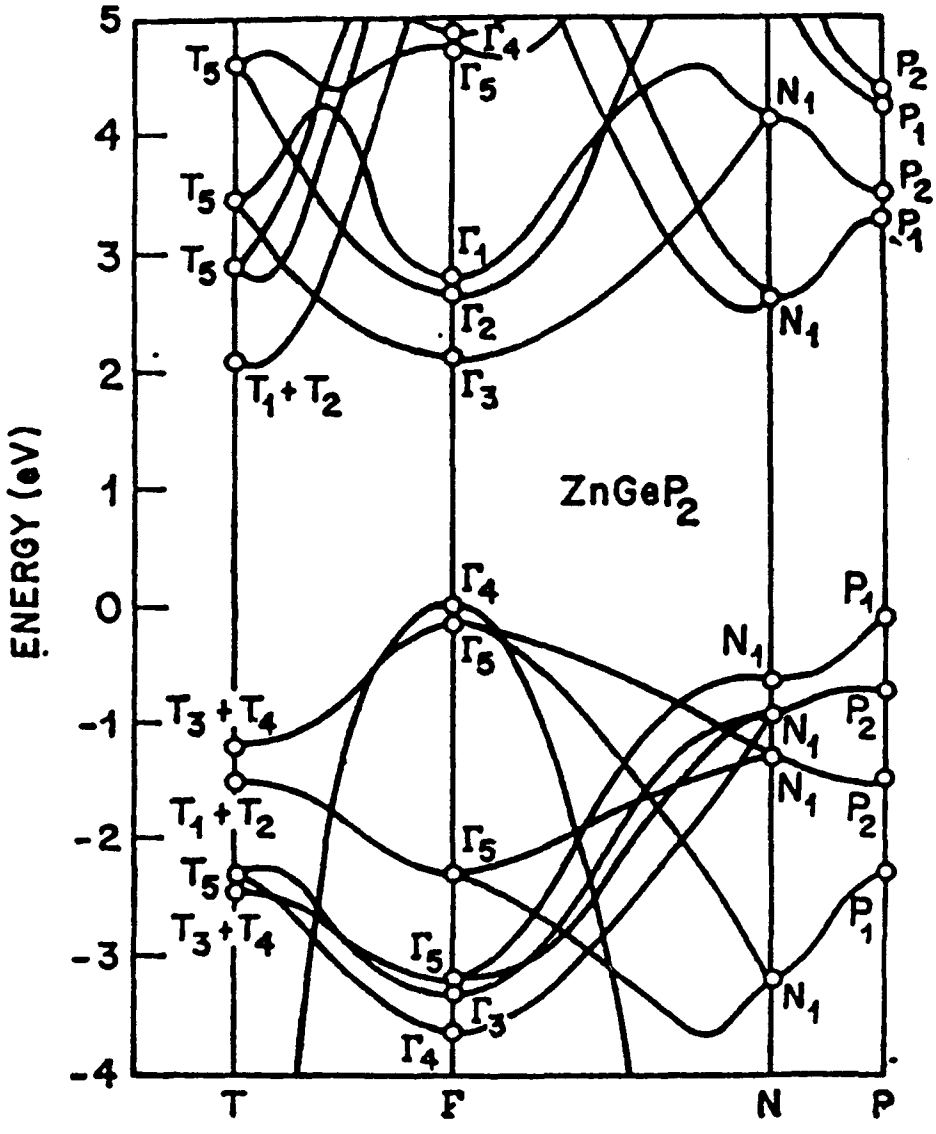

Figure 6. Band structure of $ZnGeP_2$. (Shileika, 1973:733)

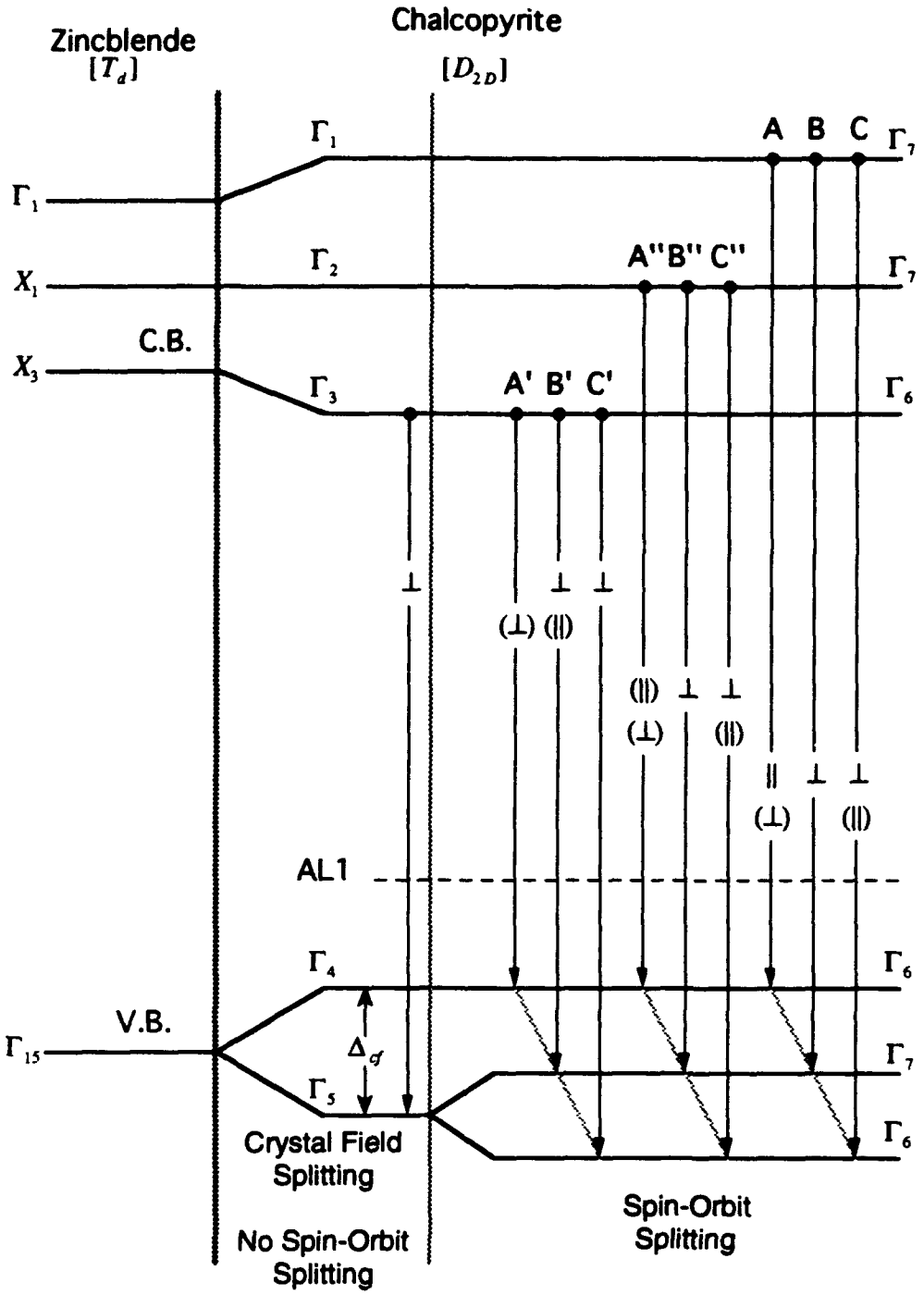

Figure 7. Bands of $ZnGeP_2$, including the spin-orbit interaction. The || and ⊥ symbols refer to the polarization of the electric field with respect to the c-axis for emitted photons. Transitions in parentheses are expected to be weaker since they are only allowed when the spin-orbit interaction is included. Primed and double primed transitions are pseudo-direct, unprimed transitions are direct. (Babonas et al., 1974:332)

4.3 Growth of $ZnGeP_2$

Many different technologies are available for the growth of semiconductors, and a wide variety of methods have been applied to the production of $ZnGeP_2$. Successful crystal growth has been accomplished using liquid metal solutions, Bridgman methods, metal-organic chemical vapor deposition (MOCVD) and liquid encapsulated Czochralski (LEC).

The liquid metal growth approach involves cooling a molten metal solution of the constituents such that the material of interest may precipitate out. Since the metals used (typically bismuth, tin, lead, or a mixture thereof) are denser than $ZnGeP_2$, the crystals grow on the surface of the metal. A serious deficiency of this method is that some of the metal is incorporated into the crystal.(Miller, 1974:685)

The Bridgman, or gradient freeze, method creates crystals of the material of interest by forming a molten quantity of the material or its constituents, and slowly cooling the liquid. The source material may be the raw elements needed, or some of the chemicals may have been pre-reacted, even the compound desired may be used. The constituents are sealed into an ampoule and placed in a furnace. The temperature is ramped up to the melting point of the material. When enough time has passed for the melt to have equilibrated, the ampoule is drawn part way out of the furnace to create a temperature gradient across the melt, and the temperature is slowly reduced further. The material will first crystallize on the cooler side of the melt, and crystallization will then proceed slowly across the whole quantity of material. (Gentile and Stafsudd, 1974:108) Both samples used in this study were grown in this fashion.

MOCVD makes use of gaseous compounds bearing the constituents of the desired material. These gasses are flowed past a heated substrate with a lattice parameter close to that of $ZnGeP_2$, such as GaP. These gaseous compounds react at the surface forming $ZnGeP_2$ and by-products, which are carried away by the flowing gasses. The gasses used

are typically dimethyl-zinc ($Zn(CH_3)_2$), germane (GeH_4), and phosphine (PH_3). (Xing et al., 1989:381)

LEC is the most complicated process, but it is capable of creating the largest crystals. A charge of $ZnGeP_2$ is placed in a crucible, and covered with an encapsulating liquid. Actually, at room temperature, neither the $ZnGeP_2$ or the encapsulant is a liquid yet. The crucible is placed within a sealed furnace and the temperature is raised to melt the $ZnGeP_2$ and the encapsulant. The space above the encapsulant is filled with high pressure argon. An axial temperature gradient is established so the encapsulant temperature is just below the melting point of $ZnGeP_2$. A rod bearing a seed crystal is then lowered to reach the surface of the melt, and the material of interest begins crystallizing upon this seed crystal. The seed crystal used could be $ZnGeP_2$, or some other material with a closely matching lattice parameter; in fact, GaP and Si were used. The rod is then slowly withdrawn, with crystal growth continuously proceeding at the interface between the grown crystal and the melt. (Hobgood et al., 1992:4030)

4.4 Previous work on $ZnGeP_2$ related to this study

Much previous work has been done with $ZnGeP_2$. It has been studied by PL, CL, and x-ray luminescence methods. A mechanism explaining the acceptor level luminescence, and the material's extrinsic near IR absorption has been described. Improvements in IR transparency have been achieved through electron beam processing and annealing. No work appears to have been published on polarized PL with $ZnGeP_2$, but it has been used to show interesting effects in similar materials.

One large study of PL from $ZnGeP_2$ examined crystals grown by differing techniques with a variety of deviations from stoichiometry and the presence of various dopants. The undoped samples showed peaks, near 1.6 or 1.3 eV, whose magnitudes varied with the stoichiometry of the sample, and the growth technique used. (Averkieva et al., 1977:453)

Another study, using CL, shows three weak features, near 1.6, 1.8 and 1.9 eV, spanning a large, broad impurity luminescence peak. This study also describes a weaker, feature rich, luminescence peak spreading from 2 to 2.4 eV, and attributed to band-to-band transitions. X-ray luminescence data showed comparable results, but with no structure seen on the weaker luminescence peak. (Gorban et al., 1984:893)

$ZnGeP_2$'s extrinsic absorption in the near-IR, and the acceptor level seen in the impurity luminescence spectrum can both be attributed to a deep acceptor level, designated AL1 (acceptor level 1), near 0.6 eV above the top of the valence band. AL1 is attributed to a native defect, possibly a germanium vacancy, or zinc on a germanium site. Long term annealing of the material near half of the melting point, and bombardment with 2 MeV electrons, have both been shown to decrease this IR absorption. It is proposed that the electron bombardment creates phosphorus vacancies which act as donors and thereby compensate the acceptor level. (Hobgood et al., 1992:4030)

The PL spectrum has been shown to vary considerably with polarization for $CuGaS_2$, a material structurally comparable to $ZnGeP_2$. (Ooe, et al., 1987:471) Recently the CL spectrum of $ZnGeP_2$ has been shown to be strongly polarization dependent. (Gregg, 1992:52)

V. Experimental Approach

The experimental setup consisted of three main subsystems: the liquid helium dewar and sample holder, the excitation laser and associated hardware, and the luminescence collection and detection equipment. Each of these subsystems and their operating procedures are described below. Figure 8 schematically represents the experimental layout.

5.1 Liquid Helium Dewar and Sample Holder

The dewar used for this study was a Janis Research Company Supervaritemp 10-liter liquid helium optical cryostat. This dewar has four chambers: the liquid helium reservoir; the sample chamber; the vacuum jacket; and the liquid nitrogen jacket.

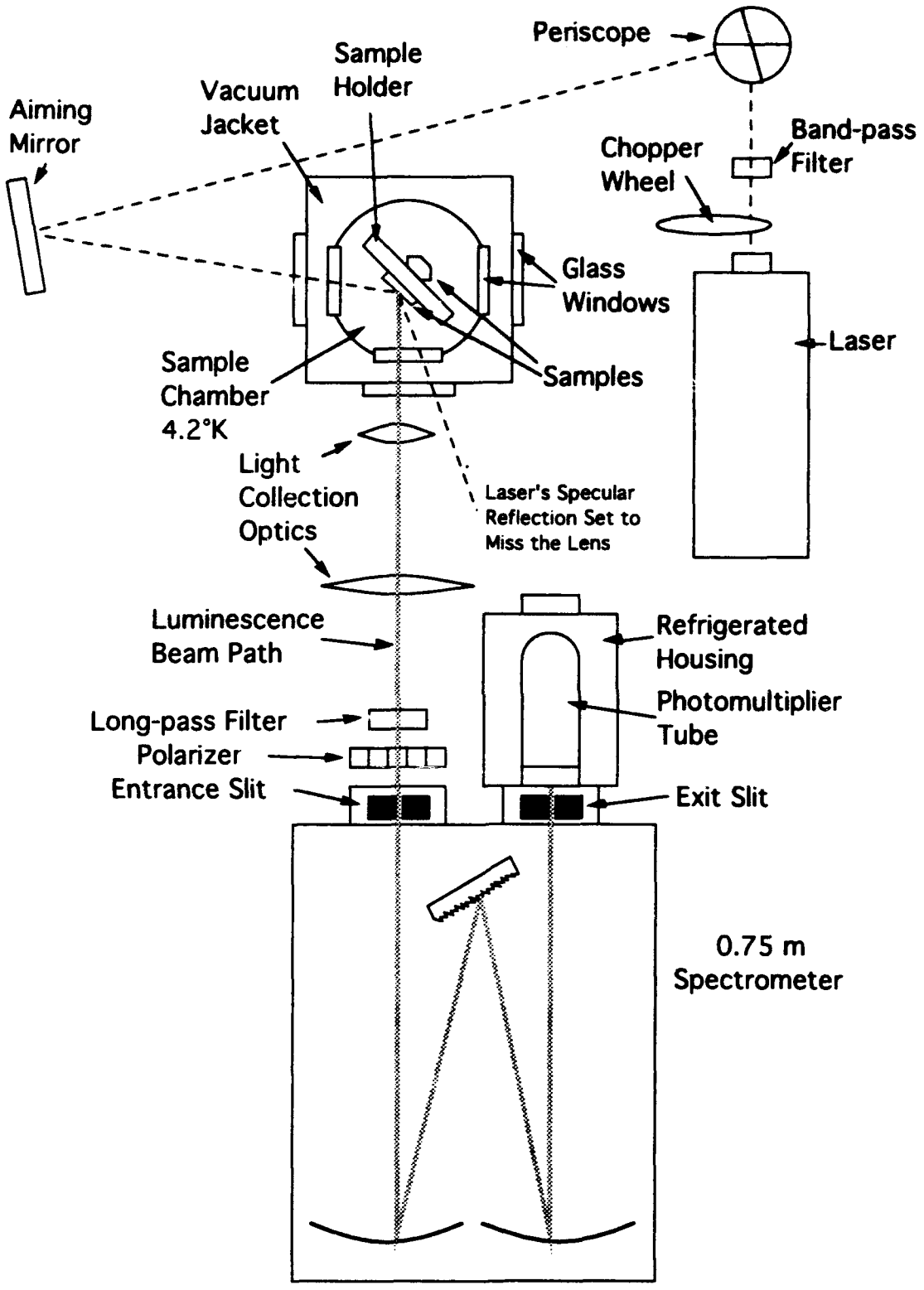

Figure 8. Layout schematic for PL measurements.

The vacuum jacket must be evacuated to at least one micro-Torr of pressure before the dewar can be cooled down. When this vacuum is achieved, the sample chamber and the liquid helium reservoir can be evacuated by starting the mechanical pump plumbed to these chambers and opening the valves connecting the pump to these chambers. The valve to the vacuum jacket is then closed, and the turbopump is allowed to spin-down. Liquid nitrogen can then be poured into the liquid nitrogen reservoir. After one hour, the turbopump and its mechanical backing pump can be shut off; after several hours, the liquid helium reservoir will have cooled to near liquid nitrogen temperature and can be filled with liquid helium. The valve between the liquid helium reservoir and the pump is shut and the reservoir is back-filled with helium gas. Liquid helium is transferred from a storage dewar to the reservoir using a vacuum insulated transfer line.

The sample chamber is cooled by opening a small needle valve which allows liquid helium from the reservoir to enter the sample chamber. While helium is being transferred, the needle valve is occasionally opened a quarter of a turn. If the pump, which is still pulling on the sample chamber, begins to gurgle, liquid helium is collecting in the reservoir. If the pump gurgles after several turns of the valve, then helium gas is in the reservoir, and the transfer rate may need to be increased by pressurizing the storage dewar to a few psi. If the pump doesn't gurgle at all, or if the needle valve cannot be turned, then a ice-block (either water-ice or frozen nitrogen) has plugged the needle valve, and the entire system must be brought to room temperature before cool-down can be reattempted. While helium transfer is progressing, an electrical helium level gauge monitors the liquid helium level in the reservoir. When the helium transfer is complete, the sample chamber can be cooled down. The valve between the pump and the sample chamber is closed, and the needle valve is opened about a full turn. Electronic gauges monitor the temperature at the bottom of the sample chamber and on the sample holder. When the temperature on the sample holder stops falling and begins to rise, the pressure in the sample chamber has reached atmospheric and prevents more liquid helium from

entering through the needle valve. A small relief valve is then opened at the top of the sample chamber to allow gravity to feed liquid helium into the sample chamber. The needle valve is adjusted to maintain a small pool of liquid helium below window level on the dewar. Some variations of this procedure are also used occasionally, however, allowing the pressure in the vacuum jacket to exceed the pressure in the helium reservoir or allowing water into the dewar where it can freeze could destroy the dewar, so great care must be exercised.

Normally, samples are mounted on the sample holder, and placed within the dewar before cool-down commences, but samples may be exchanged at any time. The sample holder is withdrawn from the chamber, the chamber is capped, and a slight overpressure of helium is used to keep the sample chamber clean. When the sample holder is warm and dry, it and the samples to be mounted are cleaned with methanol and cotton swabs. The sample is then mounted with a spot of rubber cement, using tweezers. For thin samples, it is important to use as little cement as needed, in order to prevent strain in the sample when cooled down, due to different coefficients of thermal expansion of the copper sample holder and the sample itself. Strain could change the luminescent properties of the sample. In this study, samples investigated were quite thick (>1 mm), so this would not be a problem. None the less, only a dab of cement was used on each sample. Before re-inserting the sample holder, it was rapped to verify that the samples were not likely to fall off in the dewar. The sample holder is then placed back within the dewar. The sample holder rod extends up through a gasket to the top of the dewar, thus the samples can be rotated, raised and lowered within the sample chamber to help align the laser and luminescence beams.

5.2 Excitation Laser

Two different lasers were used for this study: a Coherent Innova 300 krypton-ion laser, operating simultaneously at 350.1 nm and 356.4 nm in the ultraviolet, and an Ion Laser Technology model 5400 air-cooled argon-ion laser, which was tunable to a number

of visible wavelengths. The krypton-ion laser was capable of putting out half a watt of power, but this much was not typically used. The argon-ion laser was operated at 488.0 or 514.5 nm. Although the laser's internal power meter reported output powers as high as 40 mW, direct measurement with a power-meter indicated only 30 mW maximum. The laser beam was chopped at 92 Hz by a SRS model SR540 chopper-wheel and controller. The laser beam then traversed either a band-pass filter or a short-pass filter, possibly a half-wave plate, a periscope, a steering mirror and the dewar's windows before finally hitting the target. The filters were required to prevent strong emission lines in the plasma tube from reaching the spectrometer. When the UV laser was used, a fair amount of power was required, because the band-pass filter used only had a transmission of 17%. The band-pass filter used for 514.5 nm had a transmission of approximately 50%. The band-pass filter available for 488.0 nm had a transmission of less than 10%, so a 500 nm short-pass filter was used instead. This short-pass filter had a transmission at 488.0 nm of 70%. The half-wave plate was designed to work at both argon-ion laser wavelengths used, to optionally rotate the polarization of the laser beam. The periscope brought the laser beam up to the level of the dewar windows, and sent it on to the steering mirror. The steering mirror was used to position the laser beam precisely upon the sample, and it was verified that the laser beam's specular reflection from the sample's surface did not enter the light collecting lens.

5.3 Collection and Detection of Luminescence

The luminescence collection and detection equipment consisted of a pair of lenses, various long-pass filters, polarizers for the visible and infrared, a Spex model 1702 3/4 meter spectrometer with a 4 inch square, 1200 lines/mm grating blazed at 5000 Å, a type S1 photomultiplier tube (PMT), a Scitec lock-in amplifier, and a Zenith Z-248 computer running Labtec Notebook software to log data and control a Metrabyte analog-to-digital converter. Additional support equipment included a high voltage power supply to bias the PMT, a multimeter to monitor the PMT voltage, a refrigerated PMT housing, a

temperature control unit for the PMT housing and a nitrogen cylinder and liquid nitrogen dewar to cool the PMT housing.

The pair of lenses were used to collect the photoluminescence signal. To align these lenses, a high intensity lamp was shined upon the sample from the side of the sample chamber, the lenses were then positioned to form an image of the sample on a sheet of paper taped over the spectrometer's input port. When the lamp was removed, and the laser turned on, the diffuse reflection of the laser from the sample would also fall upon the paper. When the laser spot was seen to be on the right part of the sample, and the image of the sample fell upon the input port of the spectrometer, the coarse alignment of the system was considered complete. The chopper wheel was started, the photomultiplier housing was cooled to -30° C, the photomultiplier tube was charged to -1025 volts. A long pass filter was placed in front of the entrance slit to prevent laser light, or plasma tube emission lines from entering the spectrometer, where they could appear in the gratings second order spectrum. Unfortunately, nothing much can be done to reduce the effects of plasma tube emission lines which occur in the same wavelength range as the photoluminescence, because the band-pass filter on the laser beam is not completely successful in eliminating them. The spectrometer slit was then opened and the spectrometer was set to a wavelength where a strong photoluminescence signal was expected, typically 9000Å, for the $ZnGeP_2$ Sample. The lock-in amplifier was then turned on and set to a one second time constant; its sensitivity scale was increased until the signal was found. The phase of the lock-in amplifier was then optimized by finding the phase which made the signal go to zero and adding or subtracting 90° to reach the peak positive response. This procedure is used because it is easier to find the zero than the maximum of a noisy signal. Finally the collecting lenses were repositioned with their micrometer adjustable stages until the signal was maximized. At this point a polarizer could be placed in front of the spectrometer's entrance slit and the system was ready to take data.

To begin a data run, the computer was first programmed with the length of the run and the wavelength range to be covered, and told to wait. All the computer does is take data at a specified rate for a specified amount of time, and thus it is up to the user to insure that the information saved by the computer is indeed the data desired. The spectrometer was then rolled back to at least 50 Å below the starting wavelength and started forward at the appropriate rate. When the spectrometer reached the starting wavelength on the dial, a key is pressed on the keyboard telling the computer to start taking data. This is the only synchronization between the computer and the spectrometer. The room lights were then turned off, and data collection was allowed to proceed uninterrupted until the end of the run, when the spectrometer drive was shut off. Data runs were stored in files with sequential names. Important parameters for each run were stored in the file header, and a more complete set of run parameters were logged in a notebook.

The wavelength on the spectrometer dial is only approximately correct, so a calibration run was performed with a krypton discharge lamp to allow the wavelength on the dial to be converted to an actual wavelength. The lamp was placed between the collection lenses and centered in the luminescence beam path. The chopper wheel was placed in front of the entrance slit, and then a data run, as described above, was undertaken.

VI. Results and Discussion

Photoluminescence spectra were obtained under a variety of conditions. The polarization, wavelength, and power of the laser were varied, two different samples were used, and the polarization of the emitted light was examined. The PL results were compared to CL measurements on the same sample. Wavelength ranges where direct and pseudo-direct transitions are expected were examined. The spectra observed were related

back to the band structure of $ZnGeP_2$. Sources and magnitudes of experimental error are discussed.

6.1 Samples Investigated

Two different sample were examined in this study. Both were provided by Dr M. C. Ohmer of the Wright Laboratory's Materials Directorate, and had undergone annealing and 1 MeV electron bombardment to reduce their near-band-edge optical absorption. Sample 24d had the shape of a cube with a pair of opposite edges cut off, making it a hexagonal prism. Sample 24d was grown by the Bridgman method, and its c-axis was known to be normal to the hexagonal faces. Its composition is believed to be nearly stoichiometric. Sample 11c was a kidney shaped slab of 1.7 mm thickness, and was grown by the Bridgman technique. Its crystal orientation remains unknown, but it is suspected that the c-axis lies nearly parallel to the surface, along the length of the polished facets. The composition of sample 11c is known to be ZnP_2 deficient.

6.2 Dependence of Photoluminescence upon Polarization

The polarization resolved PL spectrum of sample 24d was taken using three different laser wavelengths: 514.5 nm, 488 nm, and multiline-UV (350.1 & 356.4 nm). The amount of laser power delivered to the sample was not always the same. About 15 mW of power was delivered to the sample at each of the two argon ion laser wavelengths, but about twice this much power (34 mW) was used with the UV laser. Two different polarizers were used as well, each with its own benefits and disadvantages. The visible range polarizer stops acting as a polarizer for wavelengths longer than 0.8 μm. The infrared polarizer is specified to cover the range between 0.8 and 2 μm; at wavelengths shorter than 0.8 μm it appears to become increasingly opaque. Since the peak of the PL signal lies near 0.8 μm, both polarizers are needed to analyze the whole spectrum.

While the thermometer at the bottom of the sample chamber reported a temperature of 3.8 K during these measurements, an additional temperature sensor located on the sample holder reported about 6 K. The temperature of the sample will be

taken to be that of the sample holder . Because the PL signal from this material is both broad and weak, the slits of the monochromator were opened rather widely to collect as much light as possible. Throughout these measurements the spectrometer slits were kept at 2 mm each. Since the dispersion of the grating in this instrument is 11 Å/mm at the exit slit, the instrument resolution was limited to 30-40 Å by the slit widths; this is equivalent to an energy resolution of about 7 meV at 0.8 μm. This resolution was still much finer than the width of any features reported for $ZnGeP_2$ in the past. To achieve a steady signal from the lock-in amplifier, the time-constant was set to 10 seconds. A post-time-constant of 1 second was used to further smooth the data. To keep the data resolution near the spectrometer resolution, the spectrometer was scanned at 250 Å/min.; this suggests a data resolution of 42 Å per time constant. Each run covered a 3000 Å range. The computer sampled the lock-in amplifier's output at 1 Hz, which was faster than required, but it did no harm, and could have been useful in applying further numerical data smoothing.

Figures 9, 10, and 11 summarize the polarization dependence data taken for sample 24d using different excitation wavelengths. Originally, it was intended that the polarization of the laser beam would be varied as well. Since it was discovered that rotating the polarization of the laser, about an axis perpendicular to the c-axis, had no effect on the PL spectrum taken with the 514.5 nm laser line this course of measurements was not pursued further. Before the common features of these figures are considered, each will be discussed individually.

When the excitation laser was set to 514.5 nm, the peak response was seen at 1.42 eV, as marked on figure 9. A subsidiary feature was seen at 1.35 eV, and a very weak feature was seen below this at 1.32 eV. There is no significant feature seen at 1.67 eV, but this energy is marked because it will be seen later that a feature is found here under more energetic excitation. When the PL is examined for polarization dependence, the first thing to note is that the visible range polarizer clearly begins to leak for energies less

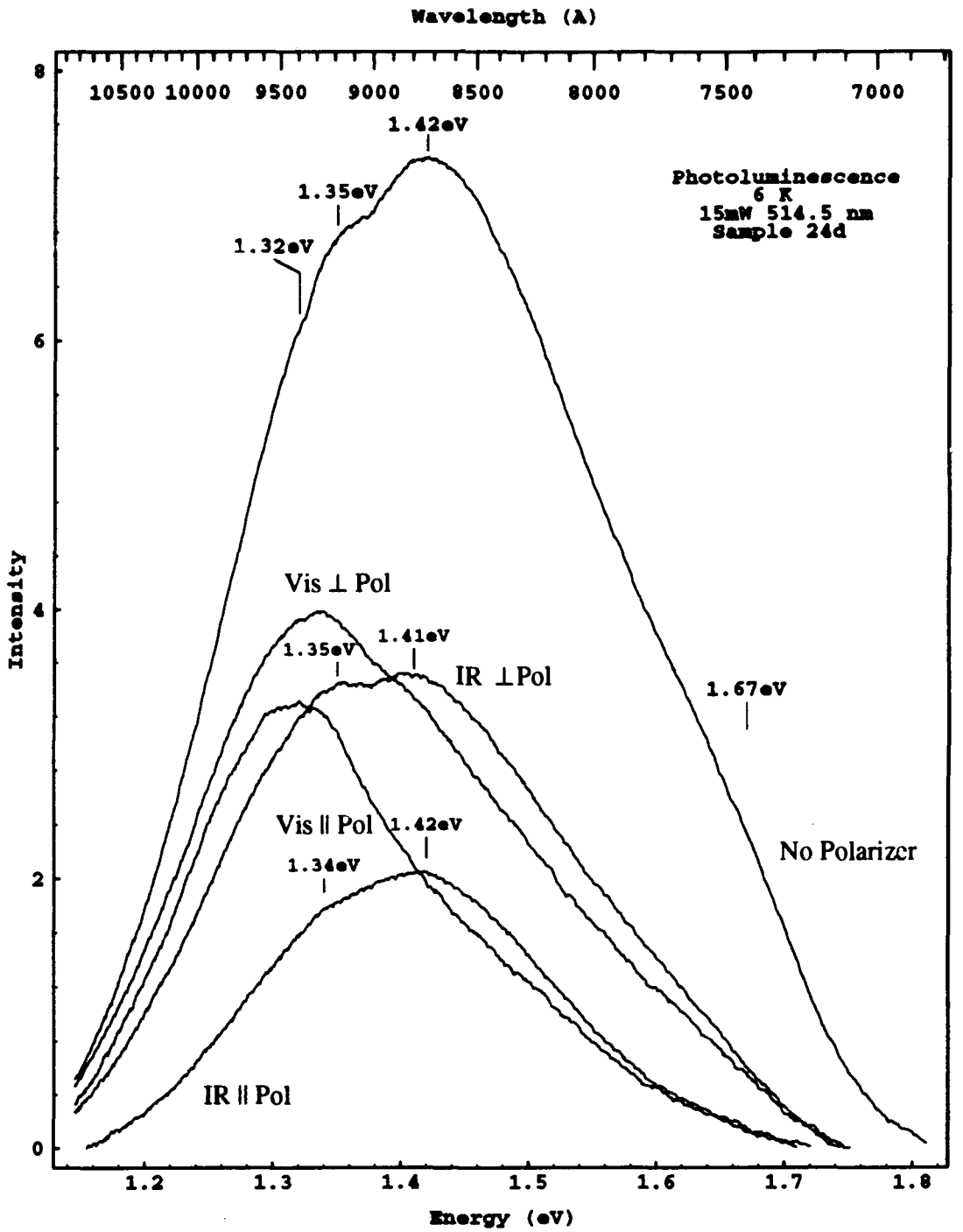

Figure 9. Photoluminescence spectra taken using 514.5 nm laser for sample 24d. Vis and IR indicate whether a visible or infrared range polarizer was used. The || and ⊥ symbols indicate whether the polarizer's pass direction was aligned along or perpendicularly to the sample's c-axis. Features marked on the spectra indicate possible transition energies.

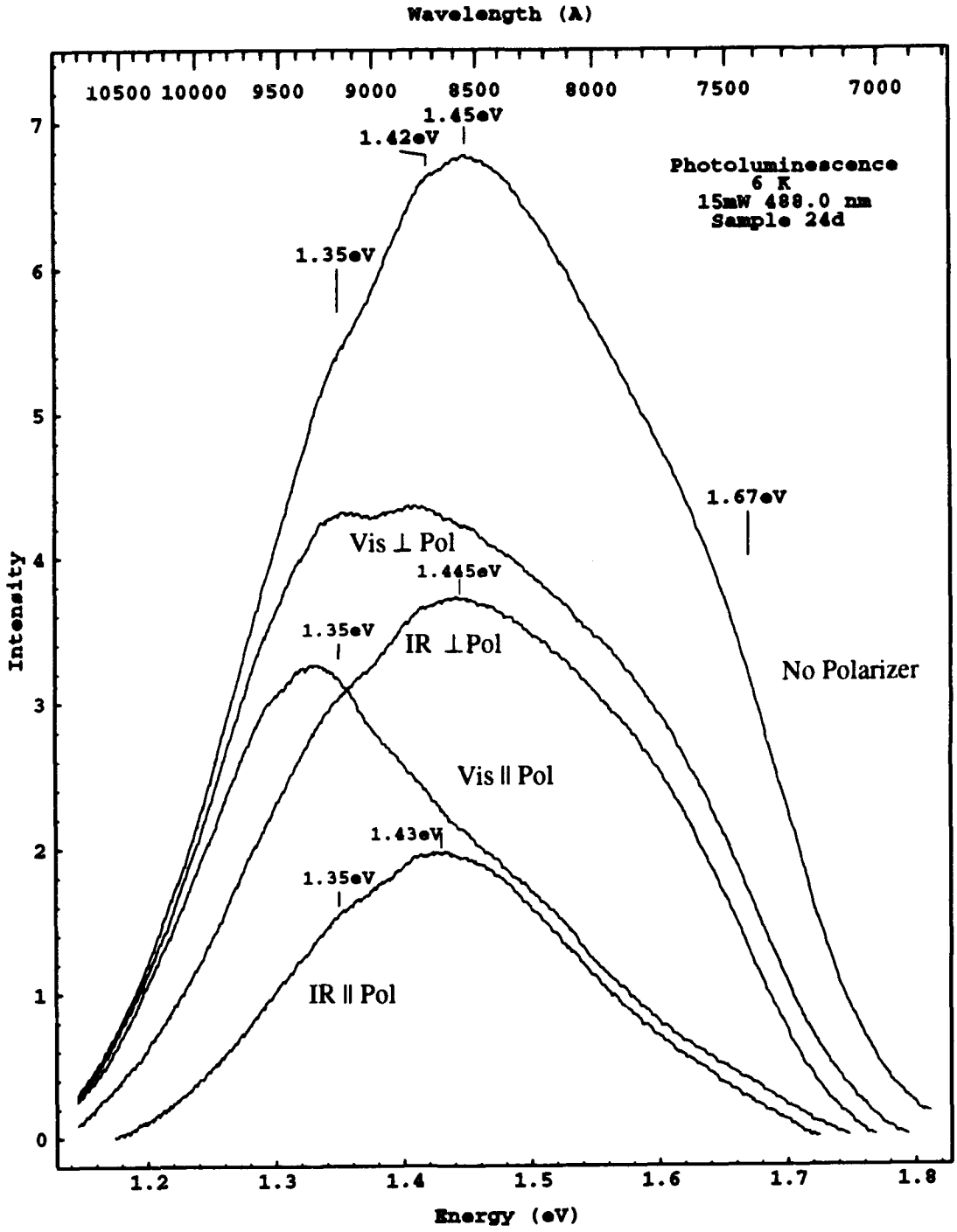

Figure 10. Photoluminescence spectra taken using 488.0 nm laser for sample 24d. Vis and IR indicate whether a visible or infrared range polarizer was used. The || and ⊥ symbols indicate whether the polarizer's pass direction was aligned along or perpendicularly to the sample's c-axis. Features marked on the spectra indicate possible transition energies.

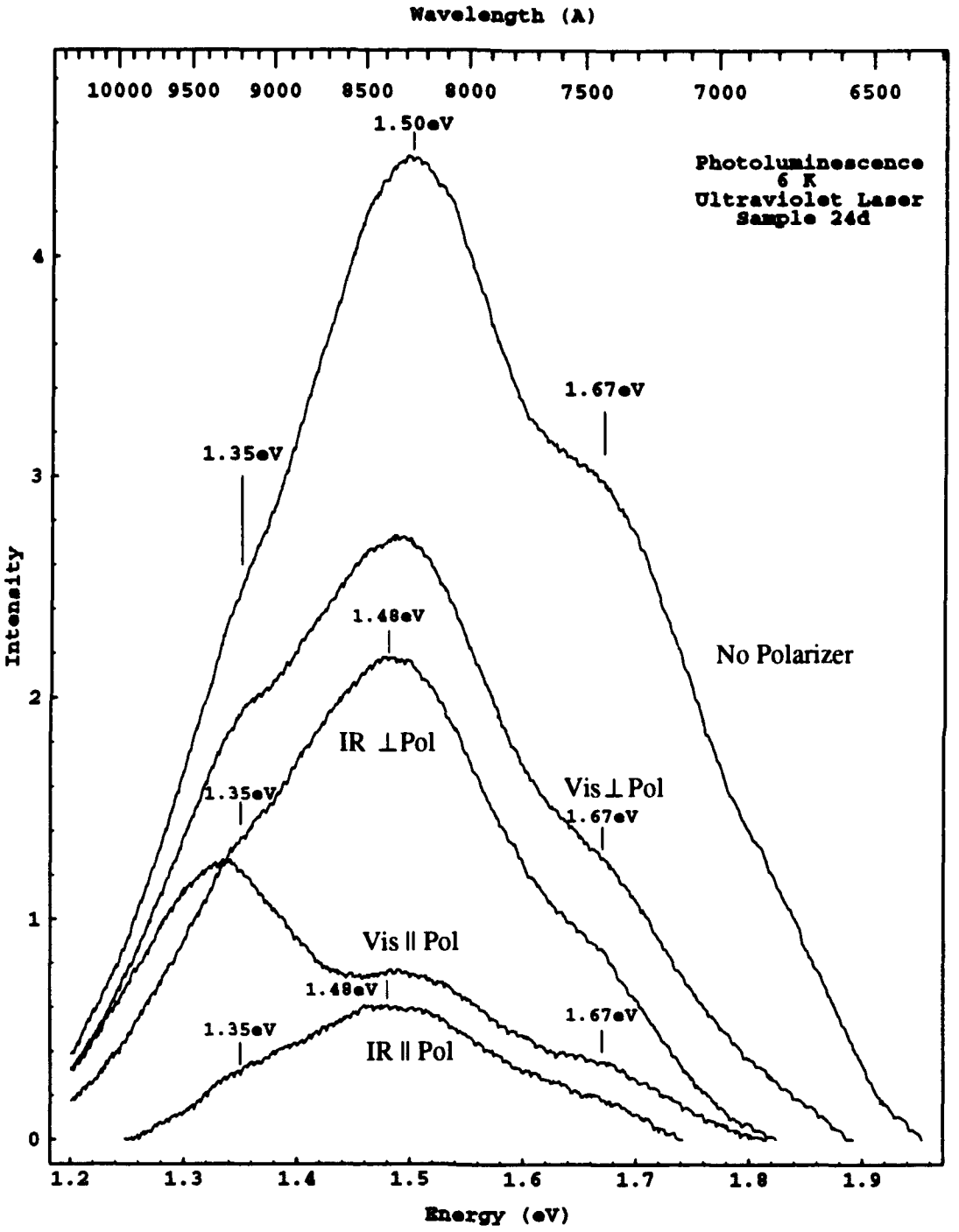

Figure 11. Photoluminescence spectra taken using ultraviolet laser for sample 24d. Vis and IR indicate whether a visible or infrared range polarizer was used. The ∥ and ⊥ symbols indicate whether the polarizer's pass direction was aligned along or perpendicularly to the sample's c-axis. Features marked on the spectra indicate possible transition energies.

than about 1.45 eV (equivalently wavelengths longer than about 8500 Å). For this reason, only the IR range polarizer gives useful data across the whole range of this luminescence signal. It is seen that emission polarized with the electric field (E) perpendicular ($\perp$) to the c-axis appears stronger than when E is parallel ($\parallel$) to the c-axis. The feature seen at 1.35 eV becomes relatively much stronger in the $\perp$ direction, and it is very weakly distinguishable in the $\parallel$ direction.

Next the laser was set to 488.0 nm, and the peak response shifted to 1.45 eV as detailed in figure 10. However, there is still a hint of a feature at 1.42 eV. The feature seen at 1.35 eV is weaker, but still present. The no polarizer curve begins to bow out noticeably near 1.67 eV. The rapid divergence of the PL with visible and IR range polarizers set in the $\parallel$ direction clearly shows the visible range polarizer beginning to leak near 8500 Å and getting rapidly worse as the wavelength gets longer. The close tracking of the IR and visible range polarizers for shorter wavelengths shows that the IR polarizer is polarizing well across the whole range, but becoming somewhat lossy at shorter wavelengths. Overall the PL is still predominantly polarized in the $\perp$ direction. The feature seen near 1.35 eV still appears to be even more strongly polarized than the main peak, however, the evidence is not so strong this time. The bowing of the spectrum seen near 1.67 eV is only clearly present in the $\perp$ direction, indicating that the light being added to the PL here is also more strongly polarized in the $\perp$ direction than the main peak.

The UV laser was then switched in, and the data depicted in figure 11 was taken. The peak response has shifted to 1.50 eV, and a very strong shoulder is seen rising at 1.67 eV. A feature still appears at 1.35 eV, but it has weakened further. The whole signal is still predominantly polarized in the $\perp$ direction. The feature at 1.35 eV still appears to be more purely polarized than the main peak, but this signal's fading strength makes this determination difficult. The degree of polarization of the shoulder at 1.67 eV is quite

difficult to judge. To help decide this issue, the data taken with the visible polarizer is replotted in figure 12, with the height of the peaks seen at 1.50 eV normalized to one.

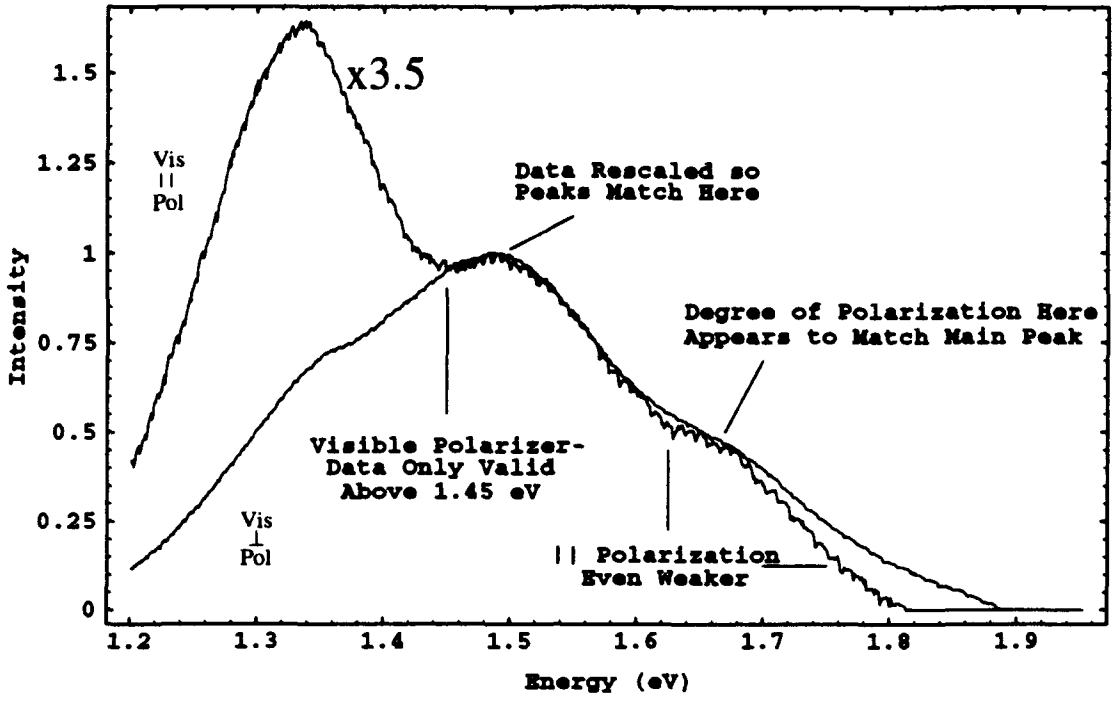

Figure 12. Rescaled comparison of polarized PL taken with UV laser for sample 24d.

The visible polarizer works properly above 1.45 eV, so the data taken with it should be accurate for both the main peak at 1.50 eV, and the shoulder at 1.67 eV. The big peak seen near 1.34 eV may not be accurate, since the polarizer is leaking a significant, and increasing, amount of the wrong polarization at this point. The feature at 1.67 eV appears on the || polarization curve with an equal relative strength to the ⊥ polarization curve. However, it may be less strongly polarized in the ⊥ direction than the main peak, because on the || polarization curve it is rising from a more rapidly decreasing tail.

Now considering the results achieved with all three laser wavelengths used, some trends are clear, but some results are puzzling. Relative to the main peaks seen in each set of PL curves, the feature seen at 1.35 eV appears to be more strongly polarized, and the feature seen at 1.67 eV seems to give ambiguous results. The data taken with the 488

nm excitation showed the feature at 1.67 eV only weakly, but it seemed to show it was more strongly polarized than the main peak. Conversely, the data taken with UV excitation showed the 1.67 eV feature strongly, and showed its polarization to be weaker than that of the main peak, but this determination was more difficult. It is also very interesting to note that the degree of polarization of the main peak increased significantly as the wavelength of the excitation was shortened. The ratio of intensities for the $\perp$ and $\parallel$ polarizations, measured with the IR polarizer, was computed for each of the three laser wavelengths. This polarization ratio exhibited a broad shallow minimum across the main peak for each laser wavelength. The measured ratios are shown in Table 1.

Laser Wavelength	Peak Position	$I_\perp/I_\parallel$
514.5 nm	1.42 eV	1.7
488.0 nm	1.45 eV	1.9
UV (350 nm)	1.50 eV	3.6

Table 1. Degree of polarization vs. laser wavelength for sample 24d.

6.3 Dependence of Photoluminescence upon Laser Wavelength

The dependence of the PL on the excitation laser's wavelength is displayed in Figure 13. This is the same data presented in figures 9-11 as unpolarized PL, normalized so each curve has the same maximum height. The weak spectral feature near 1.3 eV seen with the 514.5 nm excitation is not evident with the shorter wavelength excitations. This demonstrates how easily weak features can be washed out, and how highly convolved the underlying structure must be. The spectral feature near 1.35 eV is evident for all three excitation wavelengths, and does not appear to shift with changing excitation energy; this indicates the 1.35 eV transition is strong for all three excitation wavelengths. The main peak shifts from 1.42 eV to 1.50 eV as the excitation wavelength is shortened. The

motion of this peak suggests that there is more structure underlying this peak than can be resolved here. That is, the main peak seen at 1.42 eV with the 514.5 nm excitation is still present as a shoulder peak when the laser's wavelength is shortened to 488 nm. The feature near 1.67 eV is not apparent when the 514.5 nm line was used to excite the sample, it is very apparent when the UV laser was exciting the sample, and the 488.0 nm line gives results in the middle. Apparently, this 1.67 eV transition becomes stronger as the excitation laser wavelength decreases. The results suggest that a higher conduction band is just being reached with the 488 nm line as evidenced by a shoulder peak near 1.67 eV as shown in figure 10. The above observations and suggestions will be considered in terms of the band structure in the following section.

6.4 Dependence of Photoluminescence upon Laser Power

The laser intensity incident upon the sample can have a strong effect on the PL spectrum measured. While more laser power probably means more PL signal strength, there are several effects which should normally be avoided. Adding laser power heats the sample, which can broaden transition lines and change the bandgap. Too much laser power can also saturate transitions, changing the relative prominence of different features. To verify that the PL spectra measured were not a strong function of the amount of laser power used, and to look for the above mentioned effects, PL spectra were taken at lower and higher laser powers than those used earlier. Figure 14 shows the PL spectra taken for sample 24d at three different laser powers, using the UV laser. The UV laser was used because the available argon-ion laser was already being run near its maximum power output. The power on the sample for these three data sets are estimated to be 8, 34, and 85 mW, with a beam diameter of about 2 mm. The same three spectral features, at 1.35, 1.50 and 1.67 eV, are apparent at all three power levels.

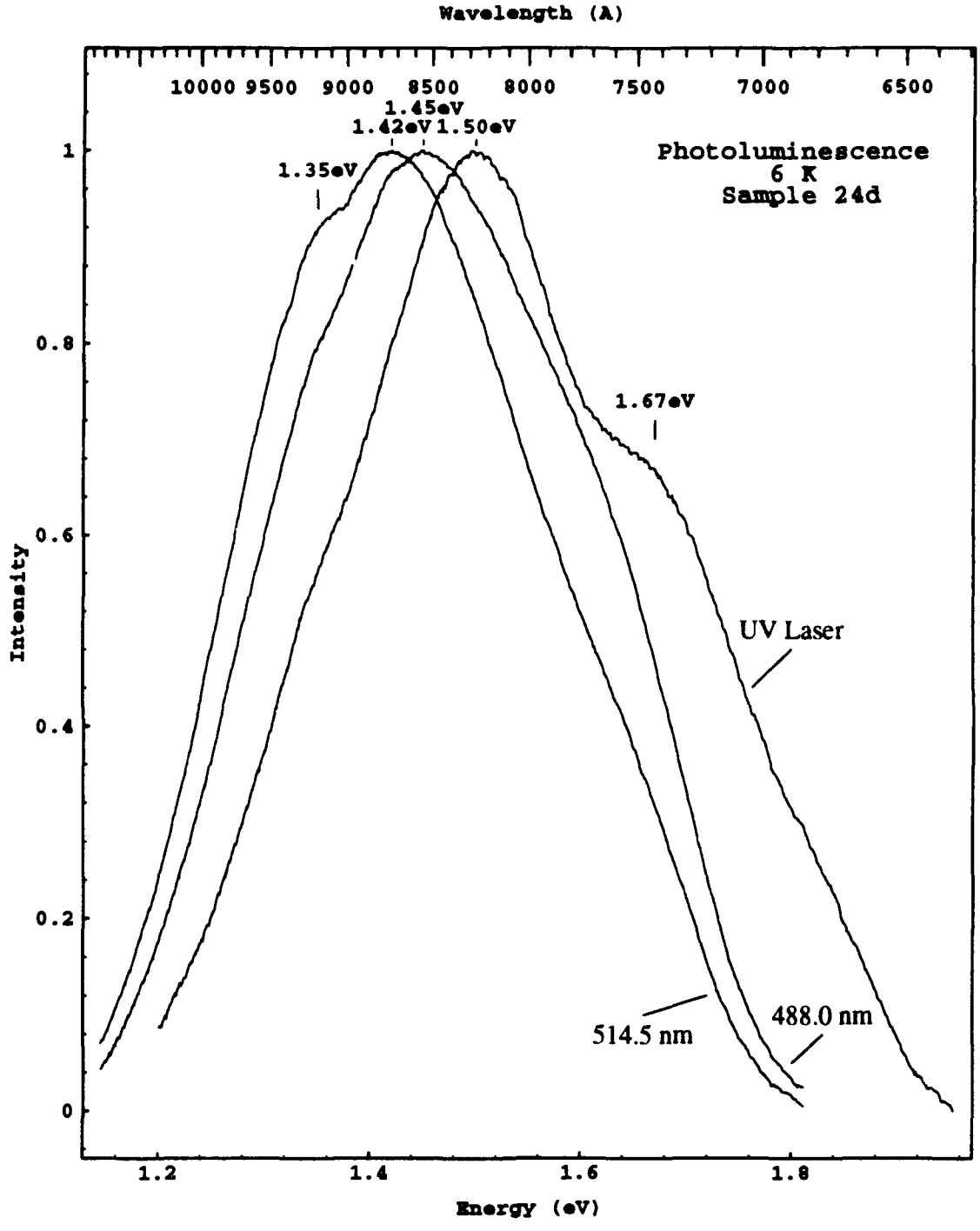

Figure 13. Photoluminescence spectrum dependence upon laser wavelength for Sample 24d.

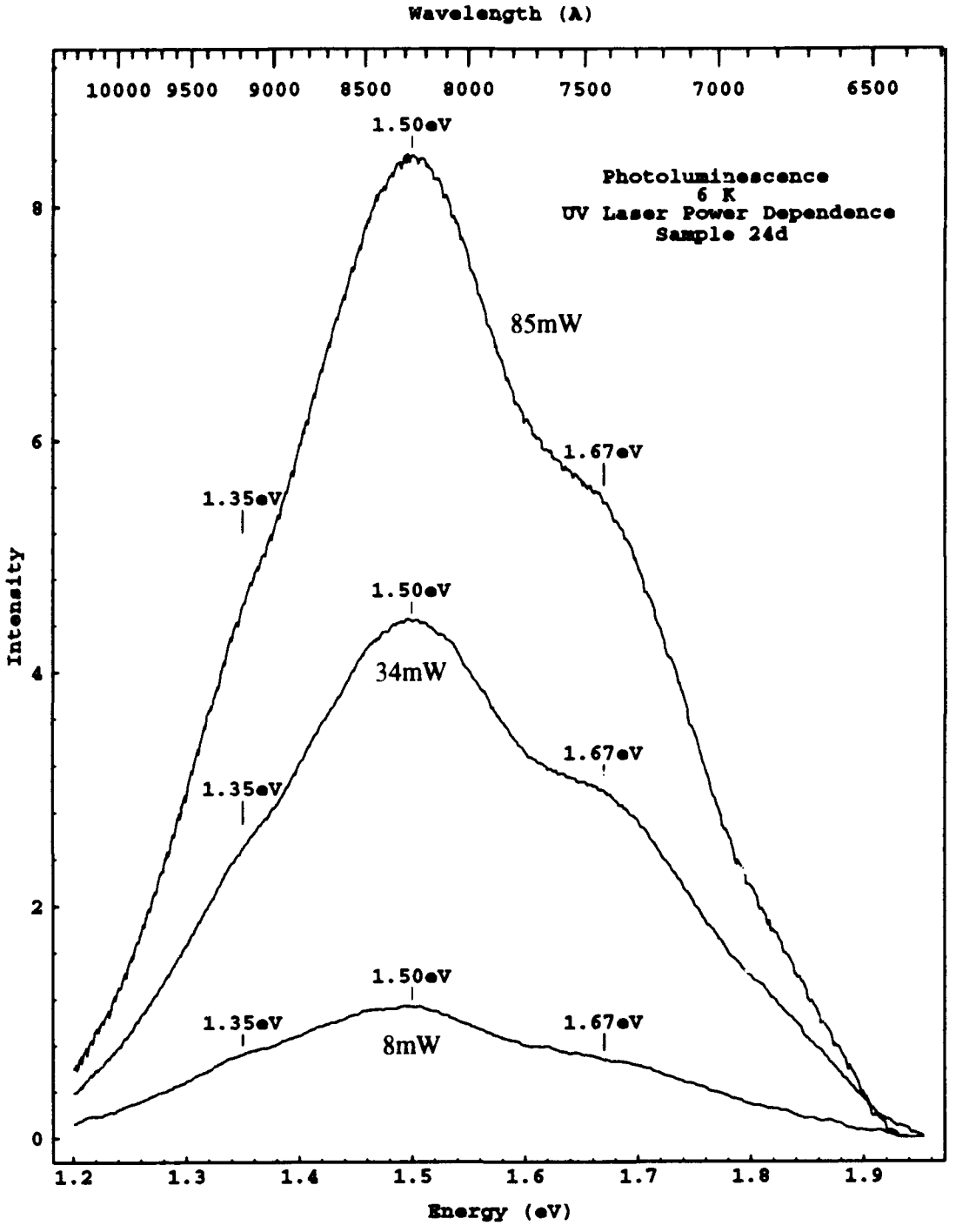

Figure 14. Effect of laser power on photoluminescence spectrum for sample 24d.

6.5 Dependence of Photoluminescence upon Sample

Photoluminescence spectra were also taken for sample 11c. Figure 15 presents the spectra taken with the 514.5 nm argon line for different emission polarizations. While the orientation of the c-axis on this sample was unknown, it was believed to lie near the plane of the sample's face, near the long axis of the sample. Thus the sample was mounted so that its anticipated c-axis would be vertical like sample 24d. While the emission was still predominantly polarized perpendicular to the assumed c-axis, the features present on the spectra for sample 24d were not evident, except the 1.34 eV shoulder peak. The peak emission was observed at 1.29 eV, which is significantly different from the 1.42 eV peak seen for sample 24d.

PL was also performed on sample 11c with the UV laser. The peak response shifted now to 1.42 eV, and a shoulder peak at 1.36 eV was evident. The signal-to-noise ratio on this run was not as good as the previous case, so perhaps a feature near 1.36 eV is just emerging from the noise. The unpolarized PL spectra for both laser excitation energies, normalized to create equal peak heights, is presented in figure 16.

6.6 Comparison between Photoluminescence and Cathodoluminescence

Cathodoluminescence spectroscopy was also accomplished on both samples discussed above, however, all the data taken was spoiled by the birefringence effect due to the sapphire window discussed in Appendix A. Nonetheless, it is useful to compare the general features of the results obtained through PL and CL. Figure 17 compares PL and CL data for sample 24d. The PL data was taken with the UV laser discussed above; the CL data was obtained using an electron beam current of 10 μA and an accelerating voltage of 4 kV. The temperature at the sample for the CL measurement was estimated to be 8-9 K, based on a temperature on the mounting finger of 4.2 K. The oscillation seen on the CL curve is at least partially artificial, so it is not possible to accurately assign a peak position, however, one of the main peaks in the CL curve appears to relate to the

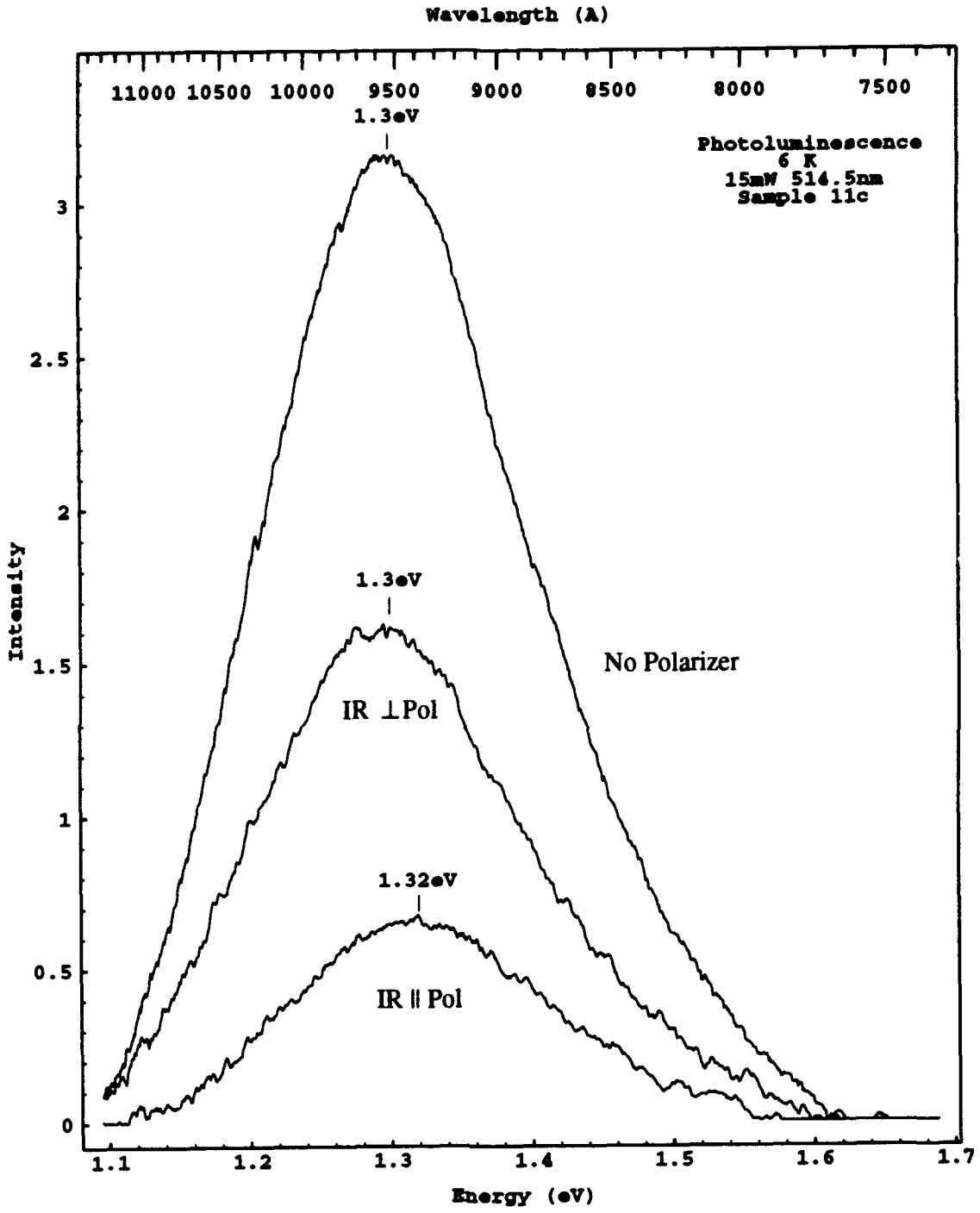

Figure 15. Polarized photoluminescence spectra for sample 11c.

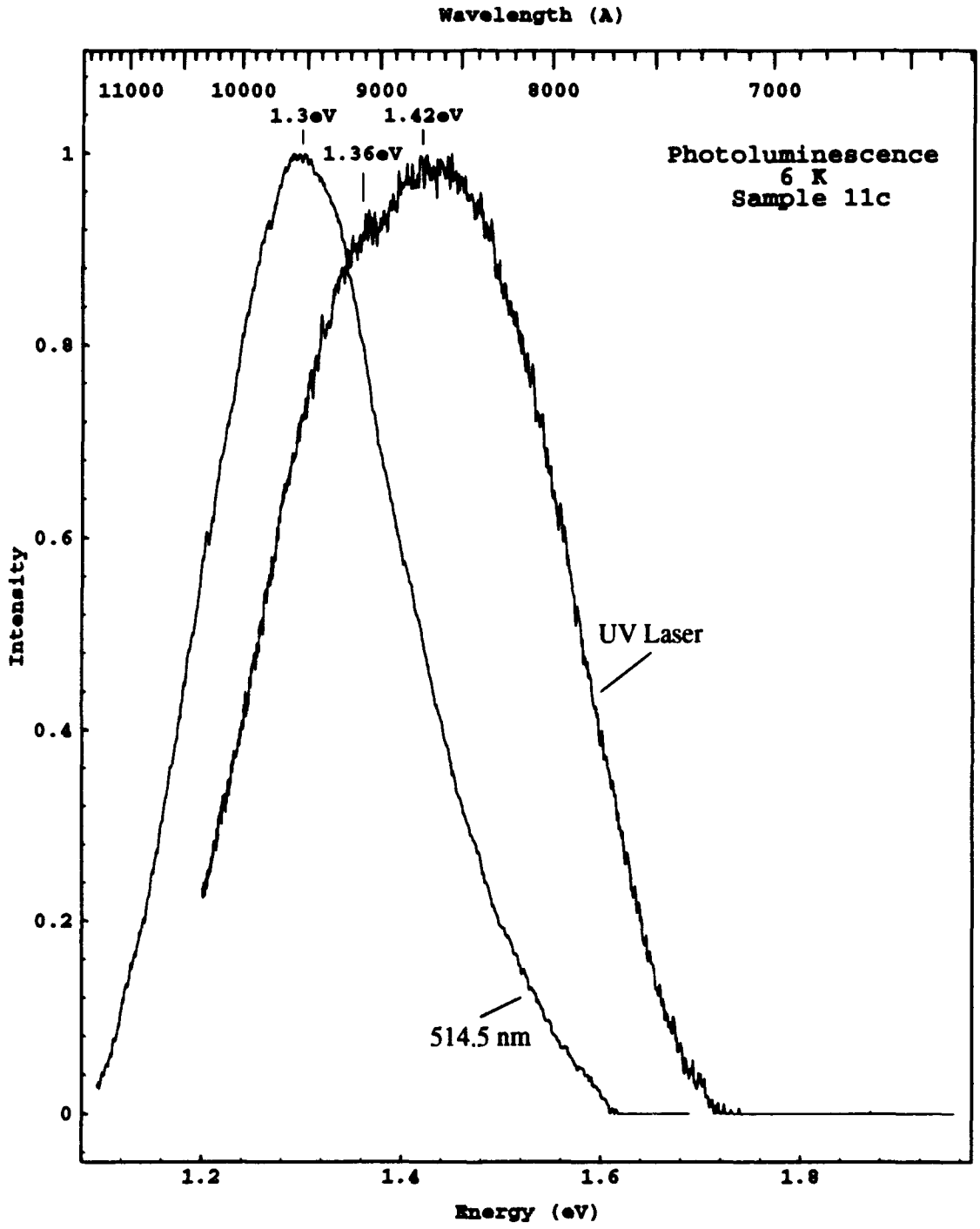

Figure 16. Effect of excitation laser energy on sample 11c.

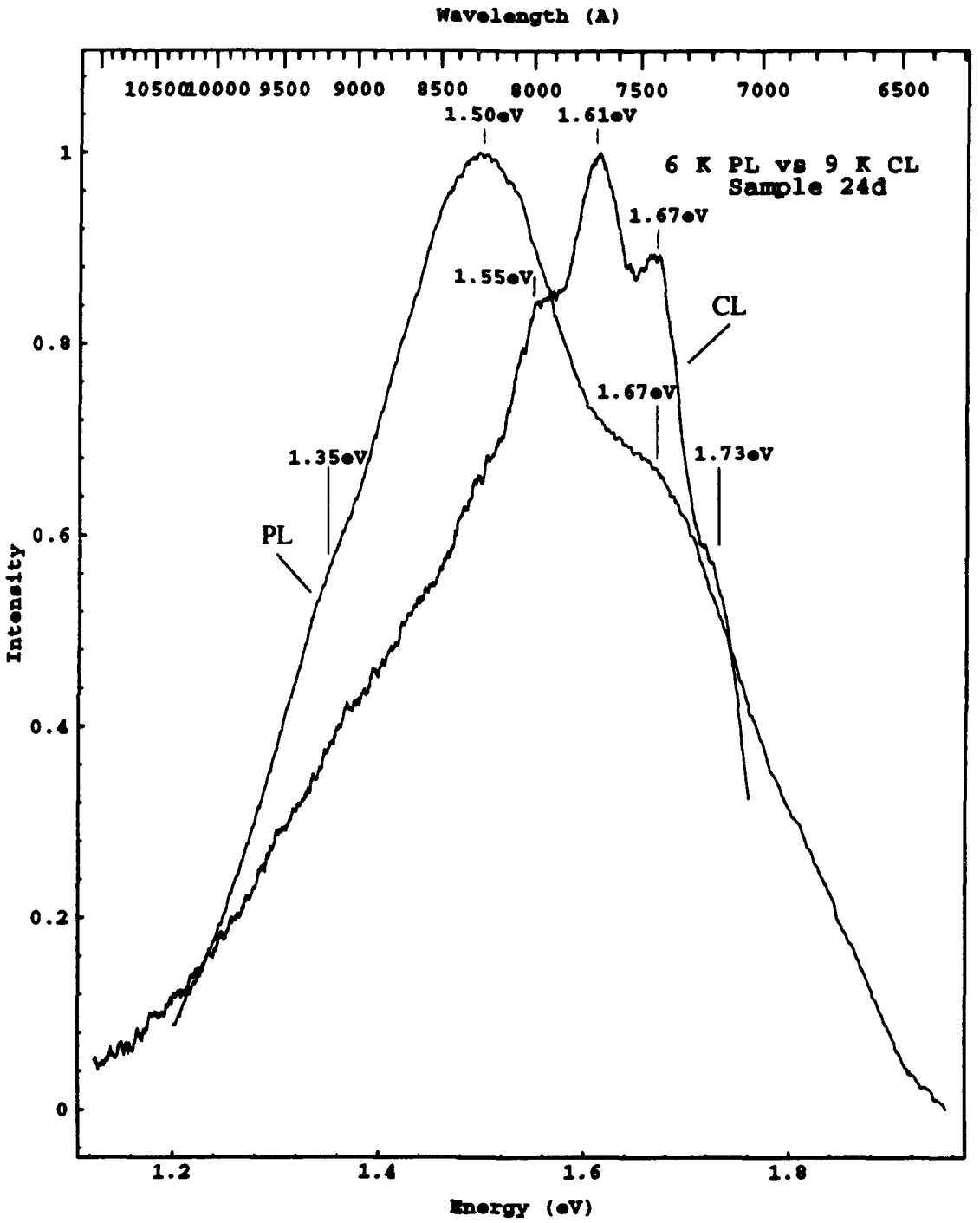

Figure 17. CL and PL compared for sample 24d.

feature seen in the PL curve at 1.67 eV. Since each electron in the electron beam carried much more energy than the most energetic photons used, the CL data can be considered somewhat like using a very short wavelength laser. Taken as such, the CL data continues the trend seen with shortening the wavelength of the laser. The peak now lies under the most energetic feature seen, near 1.62 eV.

6.7 Photoluminescence Near the Pseudodirect Transition Energy Range

The bandgap of $ZnGeP_2$ is estimated to be 2.1 eV, so near-band-edge transitions would be found near this energy. Polarization resolved PL spectra were taken over the range where near-band-edge transitions were expected with both the 488 nm and UV excitation lines. Figure 18 shows the spectra obtained with the 488 nm line. To improve the signal-to-noise ratio, the lock-in amplifier's time constant was increased to 30 seconds, with a 10 second post-time-constant, and the scanning rate was slowed to 100 Å/min. A 530 nm long-pass filter was used in front of the entrance slit, so the measured signal rapidly decreases for wavelength shorter than this. At the low end of the energy range (below 1.9 eV), the signal rapidly increases as the tail of the impurity luminescence reported above is seen. A label at 2.1 eV marks the assumed bandgap, and peaks appear near 2.08 and 2.22 eV. There was a measurable luminescence signal over the range investigated, it appeared to be not strongly polarization dependent, and well separated from the tail of the acceptor level luminescence.

Figure 19 shows the results taken with the UV laser. In this case, the time constant was set to 10 seconds with a 10 second post-time-constant. The scanning rate remained 100 Å/min. No filter was used in front of the entrance slit. No structure was seen to clearly separate itself from the noise, but there was still a luminescence signal across the range investigated. The apparent feature near 2.6 eV is probably a plasma line, since it shows no polarization dependence, and is narrower than any of the impurity luminescence features observed.

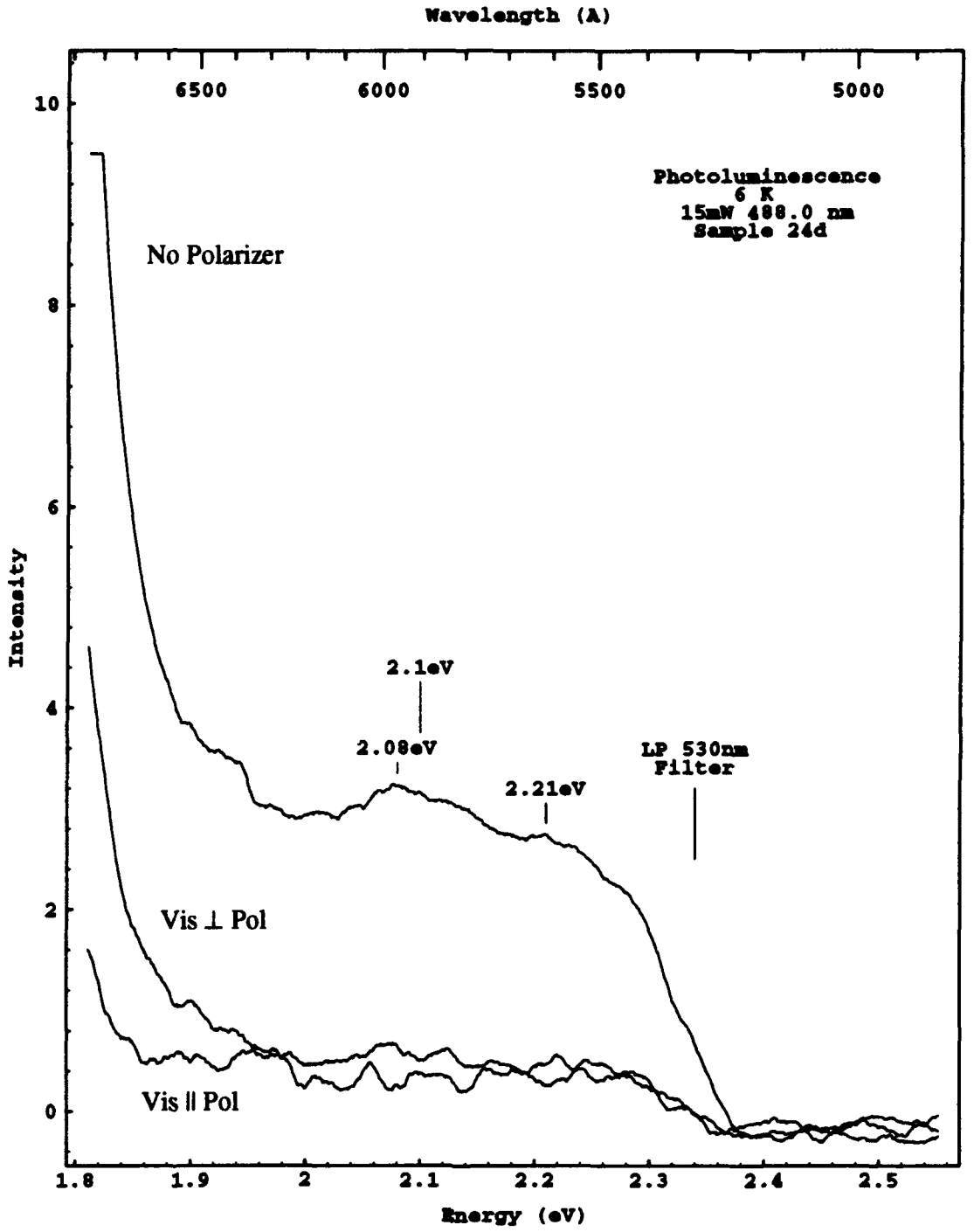

Figure 18. Polarized PL spectrum taken with 488 nm laser over expected near-band-edge emission energy range for sample 24d.

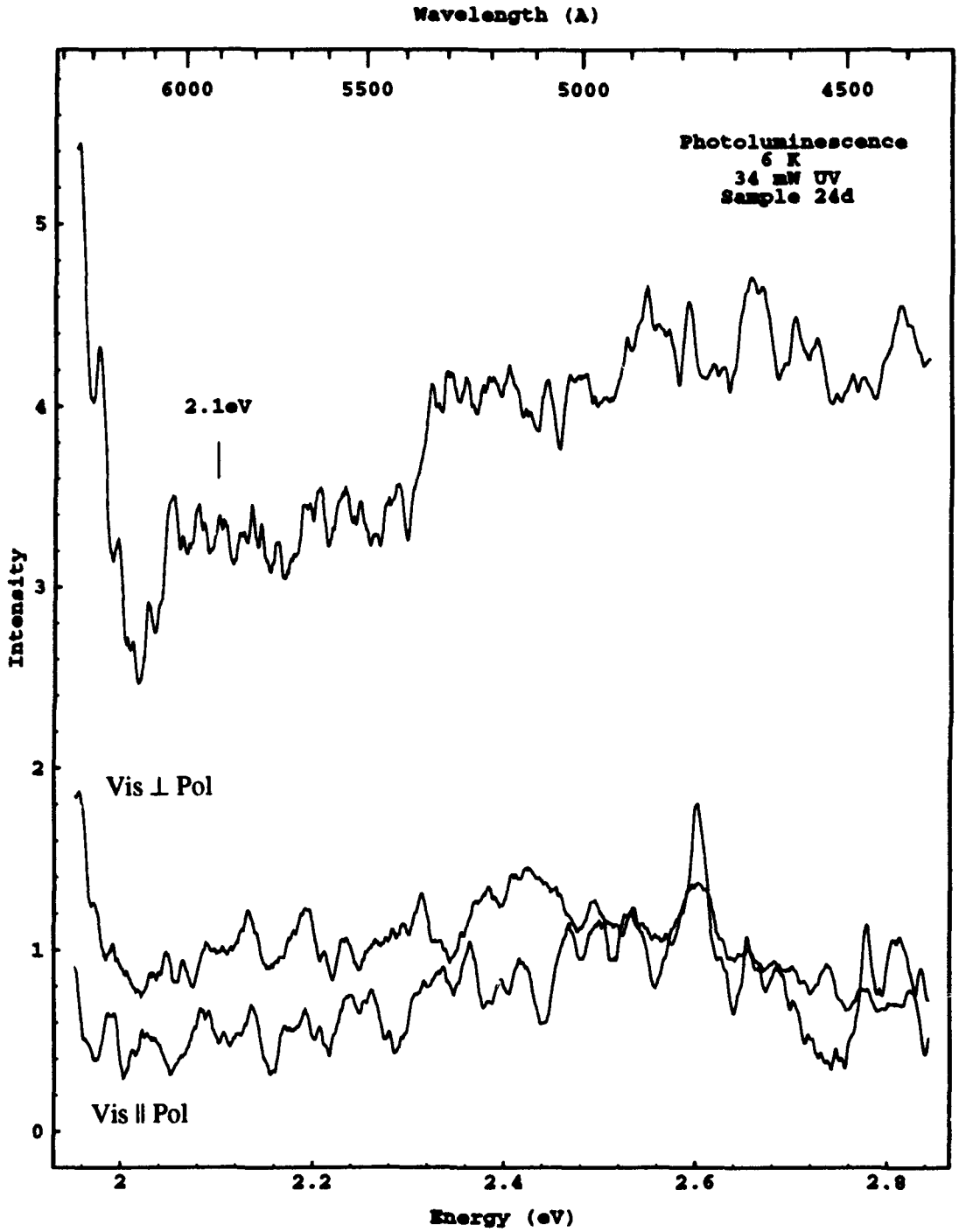

Figure 19. Polarized PL spectrum taken with UV laser over expected near-band-edge emission energy range for sample 24d.

6.8 Reconciliation of Results with Theory

The best results have been for sample 24d, so this sample will be considered here. At energies where direct and pseudo-direct transitions were expected to be found no clear evidence or distinct energy levels were found, so the data involving transitions to the acceptor level will be used to attempt to fit the spectra to the band structure. The data presented in figures 9 through 11 show three main spectral features throughout: one near 1.35 eV, one near 1.50 eV(depending on the excitation) and one near 1.67 eV. Since the relative prominence of these features varies considerably with the excitation wavelength, it may be guessed that each is associated with a different conduction band shown in figure 7. The acceptor level, AL1, is tied to the valence band, so it can have as many acceptor levels as the split valence bands, and follow the valence band selection rules (except the *k* selection rules). There were indications that the degree of polarization of the emitted light decreased for the features examined in order of increasing energy; this agrees with the selection rules show on figure 7. Each conduction band has two allowed $\perp$ and one weakly-allowed ($\perp$) transitions (again $\perp$ means that the transition where the electric field of an emitted photon is polarized perpendicularly to the c-axis is allowed and ($\perp$) means that this transition should be weak since it is only allowed when the spin-orbit interaction is considered). The allowed $\parallel$ transitions are different for each conduction level. The first conduction level has only one weakly-allowed ($\parallel$) transition to the valence band, the second has two weakly-allowed ($\parallel$) transitions, and the third has one weakly-allowed ($\parallel$) and one allowed $\parallel$ transition. Therefore it can be expected that the emitted light is always predominantly polarized with the electric field perpendicular to the c-axis, but the relative amount of light emitted with polarization parallel to the c-axis should increase for transitions from successively higher conduction levels.

An attempt may now be made to fit the features seen to the band structure shown in figure 7. Electroreflectance and wavelength modulated absorption measurements indicate that the splitting in the valence band is approximately 60-80 meV between levels

(Shileika, 1973:738). For the purpose of predicting transition energies, 60 meV will be used as the separation between the upper pair of valence bands (Γ_6-Γ_7), and 80 meV will be used as the separation between the lower pair (Γ_7-Γ_6). These measurements also show that the uppermost conduction band lies 2.46 eV above the uppermost valence band at 120 K by thermoreflectance, and that the bandgap of $ZnGeP_2$ is 2.08 eV at 77 K. Therefore the separation of the lowest and highest conduction bands shown will be taken as 380 meV. Additionally, it is estimated that the middle conduction band can be found 160 meV above the lowest conduction band. Figure 20 shows the band structure of figure 7, along with the three acceptor levels of AL1, split like the valence bands. Transitions from the conduction band levels to AL1 are marked with the same selection rules as the transitions from the conduction band levels to the valence band levels from which the AL1 splitting is derived. These transitions to AL1 are labeled AL1(*X*), where *X* represents the band-to-band transition akin to each one. Since figure 12 hints that the feature seen at 1.67 eV may be the most weakly polarized in the $\perp$ direction, it can be guessed that it represents the only strongly allowed $\parallel$ transition. The least energetic feature seen was at 1.32 eV (1.29 eV for sample 11c), so it may be assigned to the lowest energy transition, that from the lowest conduction band to the uppermost level of AL1. The increasingly energetic features seen at 1.35, 1.42, 1.45, and 1.50 eV may then be assigned to each successive transition. Choosing to place AL1 0.81 eV above each valence band makes predicted and observed energies for transitions to AL1 agree quite well for all but the lowest observed transition energy, as shown in Table 2. If the data from sample 11c is used for the lowest energy transition then there are no significant deviations between theory and experiment.

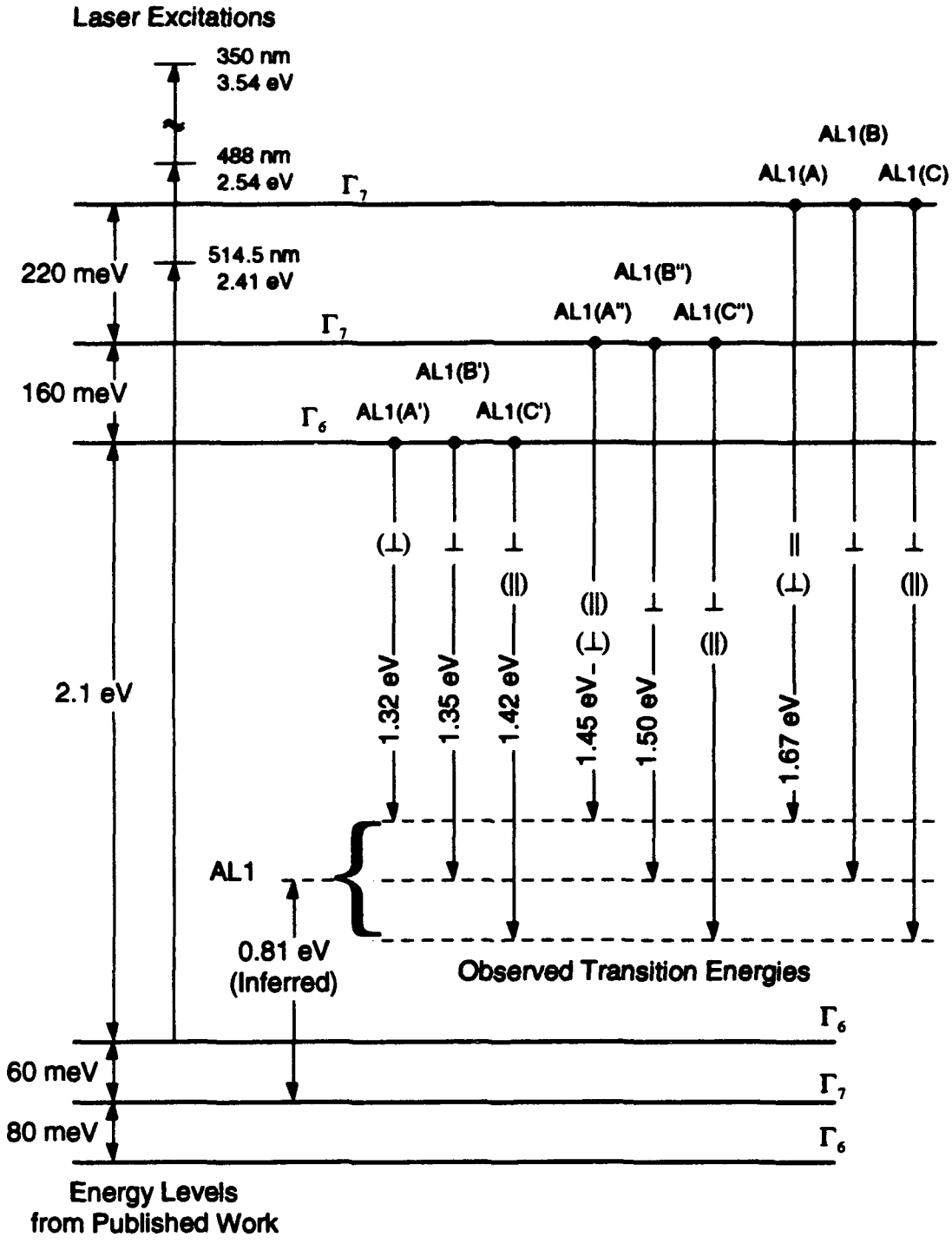

Figure 20. Proposed assignment of observed PL emissions to band structure.

Observed Feature	Transition Label	Predicted Energy	Prediction Error
1.32 eV*	AL1(A')	1.29 eV	-30 meV
1.35 eV	AL1(B')	1.35 eV	0 meV
1.42 eV	AL1(C')	1.43 eV	10 meV
1.45 eV	AL1(A")	1.45 eV	0 meV
1.5 eV	AL1(B")	1.51 eV	10 meV
Not Seen**	AL1(C")	1.59 eV	-
1.67 eV	AL1(A)	1.67 eV	0 meV
Not Seen	AL1(B)	1.76 eV	-
Not Seen	AL1(C)	1.84 eV	-

Table 2. Comparison between predicted and observed transition energies. Based upon placing AL1 0.81 eV above valence band. *Figure 16 shows a peak at the predicted energy, this transition may dominate for sample 11c. **The bowing of the curves in figure 10 could be explained by a tranistion at 1.58eV.

Considering the range of reported values for the band splittings, and the difficulty assigning peak locations which involve broad signals and steep slopes, this suggested feature assignment is well within the anticipated error bounds. In fact, other reasonable feature assignments are possible, if different values are chosen for the band splittings; the above assignment is based upon what appears to be the most reliable data.

6.9 Sources of Error

There are many potential error sources associated with the experimental results presented above. The wavelength scale, the system's wavelength response, the actual temperature of the sample, the assignment of feature locations, and the geometry of the experimental setup all could affect the accuracy of the above results and determinations.

The accuracy of the calibration and the repeatability of wavelength scan are bound to introduce some errors into the wavelength scale used for each data run. Judging from the calibration curve and the scan rates used, this error should be less than 10 Å. Since

this value is much smaller than the spectrometer resolution, due to the use of wide slits, and since the features seen were broader than the spectrometer resolution, wavelength errors as large as 10 Å would have had an insignificant effect on the data taken.

The systems response to different wavelengths of light can skew the sizes of observed features, possibly making their peak wavelengths appear to be different than they actually are. The main source of this error would be the responsivity of the PMT. When a blackbody with a known spectral radiance was used to calibrate a similar system, using the same type of PMT, it was found that the system response curve was relatively flat for energies above 1.3 eV (Gregg, 1992:89). Thus, it can be assumed that the system response does not strongly bias the above results.

The actual temperature of the sample is difficult to determine. The transducer on the sample holder reported 6 K, but the laser beam was providing heat directly to the sample, so its temperature could have been higher. Since the sample was closer to the liquid helium at the bottom of the sample chamber than the temperature transducer, its temperature could have been lower as well. The PL data, taken with the UV laser at different power settings, shows that whatever the actual sample temperature may have been, sample heating by the laser had little affect on the PL seen.

The assignment of energy values to features seen in the spectra is difficult to do accurately. The locations of the peaks were easier to determine, despite their breadth, so it is estimated that these locations were placed within ±5 meV accuracy; this is comparable to the instrument resolution. Assigning an energy value to the feature seen at 1.67 eV was more difficult. It is estimated that this transition is assigned with an accuracy of ±10 meV, since moving the marked transition by more than this amount makes it clear that the label does not align well with the feature. If there is more than one strong transition making up this feature, the error could easily be much larger.

The path of the laser beam to the sample, and the path from the sample to the spectrometer are approximately 90° apart; this makes it impossible to orient the sample

normally to the spectrometer. The optical transmission coefficients from the surface of the sample into the air can be expected to be greater for light polarized in the plane of the incidence than for light polarized perpendicular to the plane of the interface (Hecht, 1987:98). Due to the orientation of the sample, this effect would artificially increase the degree of polarization observed. Since the analysis above is based upon the relative degree of polarization between different spectral features, it is not necessarily a problem. Unfortunately, since the index of refraction is wavelength dependent and quite large (Boyd et al., 1974:301), this could have affected the above results. An additional complication is the fact that the PL was generated within about a wavelength of the surface of the sample, making any transmission coefficients which may be calculated from a ray optics picture dubious. One mitigating factor is the CL data, which was taken with the sample surface normal to the spectrometer, and which did show the luminescence to be preferentially polarized.

VII. Conclusions

The PL spectrum of $ZnGeP_2$ is seen to be dominated by transitions from the conduction bands to the acceptor level AL1. The emitted light is strongly polarized perpendicularly to the material's c-axis, and features are seen in the spectrum at three principal locations. These features can be assigned, with good agreement to published band splittings, if the acceptor level AL1 is placed 0.81 eV above the valence band. This assignment also agrees with the predicted polarization dependence of the underlying transitions. The clarity of the features seen with sample 24d exceeds that of previous results, implying that this sample may be the best material produced so far. No discernible spectral features were found in the region where near-band-edge transitions were expected, but these transitions are expected to be weak. Sample 11c, which was also studied, showed a broader and more featureless spectrum, suggesting that it may not be of the same quality as sample 24d. Since this sample's crystallographic axes are not

known with certainty, sample orientation may also be a strong factor influencing the measured spectra.

VIII. Recommendations

Additional experimentation is needed to help verify, and perhaps improve upon the results and determinations presented above. CL and PL with enhanced experimental layouts, using these and other samples, could help reveal more details of the band structure.

The most pressing need is for CL spectra to be reaccomplished (again, for reasons discussed in appendix A, the CL data taken was distorted). Since the electron beam excitation results in luminescence predominating from the upper conduction band, perhaps the splitting of AL1 will be more apparent, since the uppermost conduction band is relatively well separated from the other two conduction bands.

If additional PL data were desired, the experimental layout should be revised to pass the laser beam, and the luminescence signal through the same window on the cryostat, so the sample's facet may be aligned normally to the detector. Interesting results might be achieved using more excitation wavelengths. An excitation wavelength below 5905 Å (2.1 eV), but above 5487 Å (2.26 eV) should only have sufficient energy to excite electrons to the lowest conduction band. This would hopefully better reveal structure in the low energy portion of the impurity PL spectrum, and would help verify the identification of transitions which originate from the lowest conduction band.

It would be interesting to examine a sample both before and after electron beam bombardment. This could help elucidate the mechanism by which the electron bombardment lowers the sample's near-IR absorption. Since the electron beam carries enough energy to displace atoms in the lattice (Hobgood, 1992:4030), changes in the concentration of donors and acceptors sufficient to change the impurity luminescence might be expected.

Appendix A - Experimental Artifacts in CL Data

CL and PL data taken using the equipment in the CL lab showed strong, regularly spaced peaks across the luminescence spectrum. This structure was due to the interaction between the strongly polarized luminescence signal, the birefringence of the sapphire window on the sample chamber, and the polarizer used to analyze the spectrum. For certain wavelengths of light, the sapphire window has a whole number of waves of retardation, so it would pass light unaffected. For other wavelengths of light, the window has a half-wave more than an integral number of waves of retardation, so the polarization of incident light would be rotated by twice the angle between the fast axis of the window and the polarization vector of the light. The polarization of a strongly polarized beam passing through the window varies from unaffected, through elliptical polarization states, to rotated by some amount, and back through elliptical polarization to unaffected as the wavelength of the signal is examined. When this light is analyzed by a polarizer, a signal will be seen which oscillates with wavelength. Since this effect will not be seen if the signal is unpolarized, or the polarization falls upon the fast or slow axis of the window, sometimes this effect was not seen. Since the grating in the spectrometer has a polarization dependence of its own, sometimes this effect was noticeable even without a polarizer in the beam.

Because of this effect, the data taken with this equipment must be used carefully. This data could be used to place a lower bound on the degree of polarization of measured luminescence, and it could be used to decide approximate peak locations in luminescence signals, but any structure which may have been on this data appears to be unrecoverable. Figure 21 shows a typical CL spectrum, along with the results of measuring the transmission of the window, with a polarizer in front of it, on a spectrophotometer whose lamp emits partially polarized light. The regular peak spacing appears clearly on both sets of data. The sapphire window flange partially blocked the entrance port on the

spectrophotometer, and the degree of polarization of the lamp in the spectrophotometer varied considerably with wavelength.

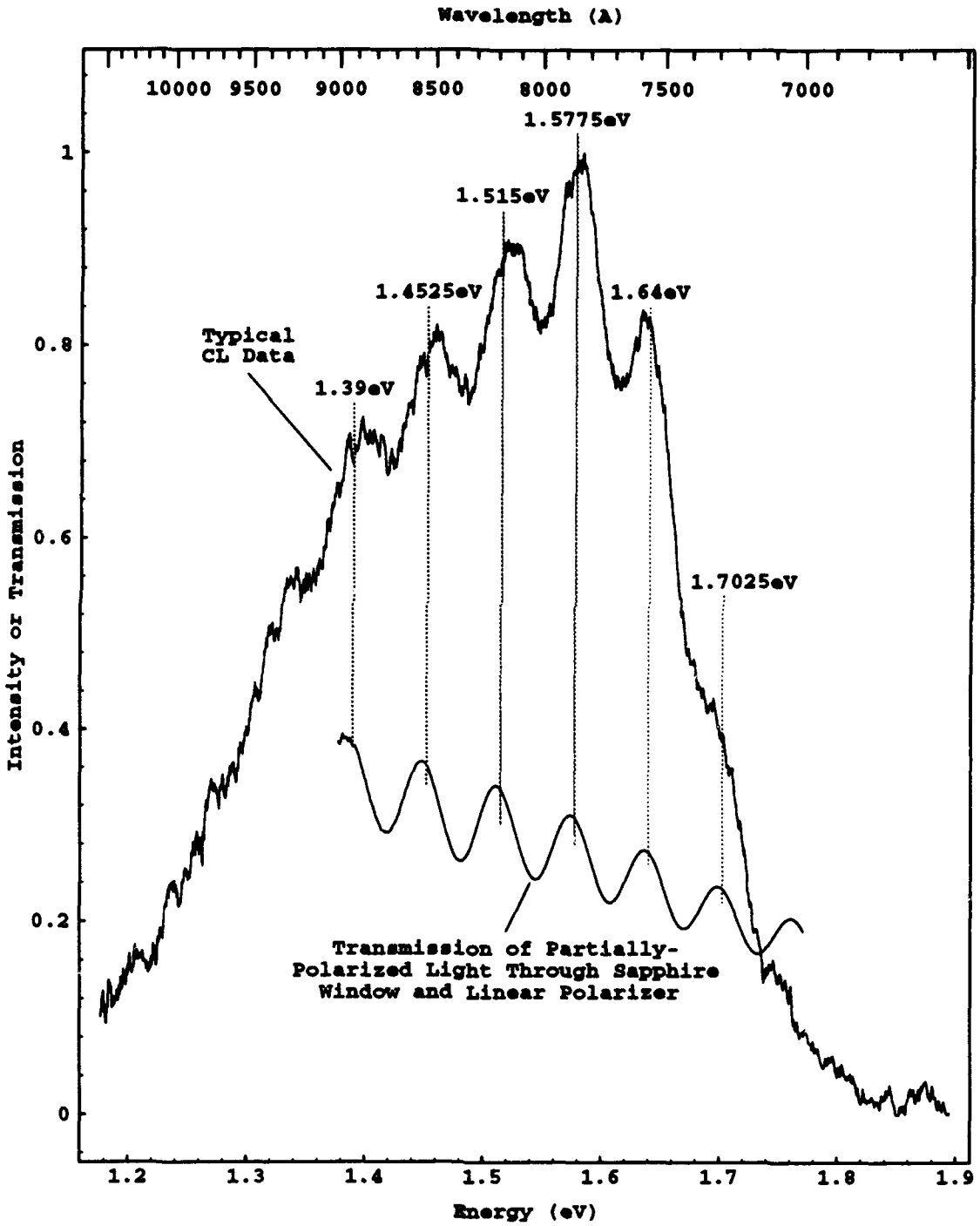

Figure 21. Comparison of polarized CL data with polarized sapphire window transmission.

Appendix B - Calibration of the Spectrometer

The process of calibration the wavelength scale on the spectrometer was described above. This appendix presents the data actually used to make this calibration. Figure 22 shows the spectrum taken as a function of the spectrometer's dial reading. The breadth of the spectral features seen is due to the wide slit spacing and the long time constant used on the lock-in amplifier. They were chosen to match those used for luminescence data collection. The width of any of the singlet lines is easily seen to be much smaller than any features seen on the luminescence spectra, thereby verifying the stated resolution of the instrument configuration used. Table 3 correlates actual line wavelengths with the spectrometer dial setting where each appeared. Figure 23 shows the error of the wavelength dial vs. actual wavelength, along with a straight-line least-squares fit to the data shown. This least-squares fit states that the actual wavelength may be computed from the dial wavelength by

$$\text{Actual (Å)} = 0.9938696 * \text{Dial (Å)} - 111.275 .$$

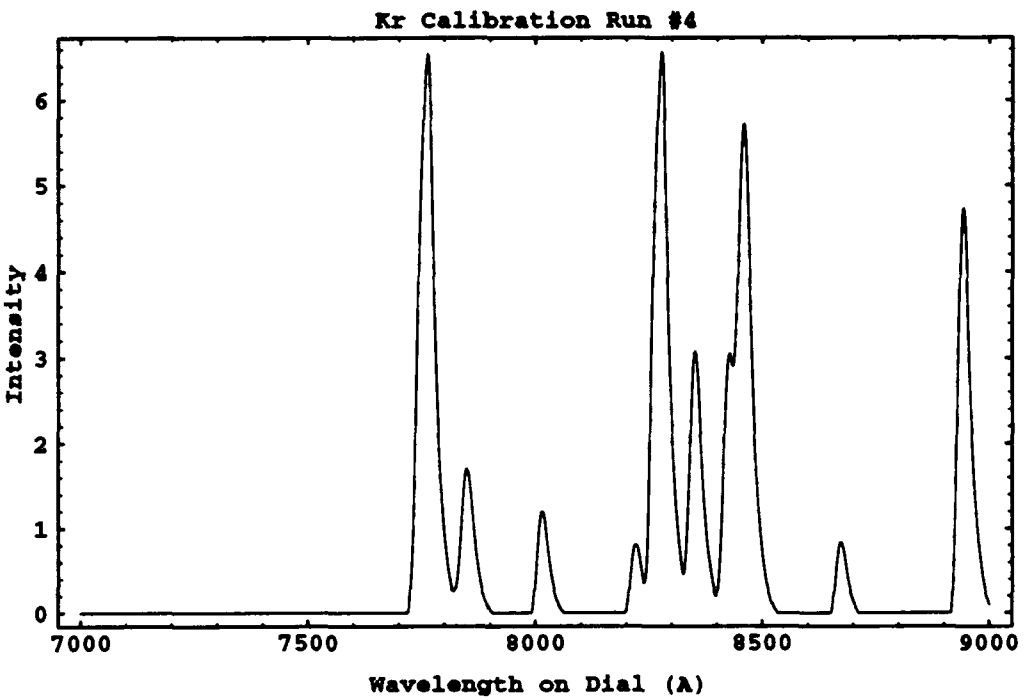

Figure 22. Krypton lamp calibration spectrum for spectrometer.

Dial Setting	Actual	Dial - Actual
7763.33	7601.5	161.833
7850.0	7694.5	155.5
8015.0	7854.8	160.2
8220	8059.5	160.5
8278.33	8112.9	165.433
8351.67	8190.1	161.567
8428.33	8263.2	165.133
8460.	8298.1	161.9
8671.67	8508.9	162.767
8943.33	8776.7	166.633

Table 3. Dial settings, actual wavelengths, and their difference for Kr calibration run on 0.75 m spectrometer.

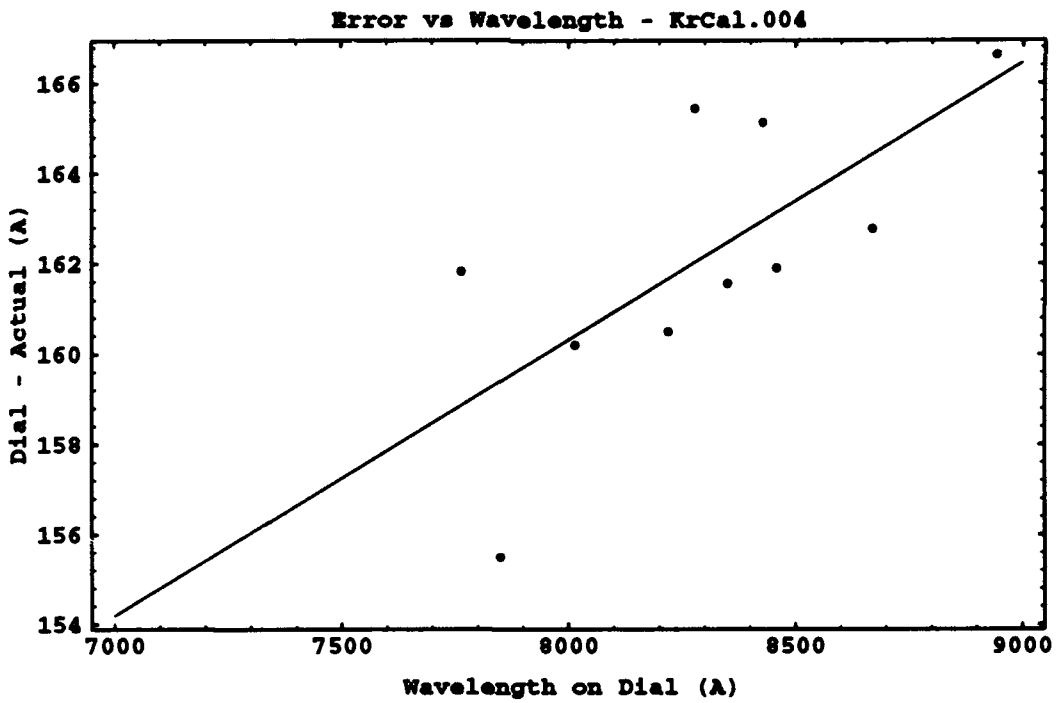

Figure 23. Wavelength error vs. spectrometer wavelength reading for calibration run.

Bibliography

Andreev, Yu. M. et al. "Second Harmonic Generation from DF Laser Radiation in $ZnGeP_2$," Soviet Journal of Quantum Electronics, 22: 1035-1046 (1992).

Averkieva, G. K. et al. "Photoluminescence of p-Type $ZnGeP_2$ Crystals," Physica Status Solidi (a), 39: 453-457 (1977).

Babonas, G. et al. "Wavelength-Modulated Absorption Spectra of Pseudodirect Bandgap $A^2C^4C^5_2$ Compounds," Physica Status Solidi (b), 62: 327-334 (1974).

Boyd, G. D. et al. "Linear and Nonlinear Optical Properties of ZnGeP2 and CdSe," Applied Physics Letters, 18: 301-304 (1974).

Budni, P. A. et al. "Efficient, High Average Power Optical Parametric Oscillator Using $ZnGeP_2$," OSA Proceedings on Advanced Solid-State Lasers, 13: 380-383 (1992).

Gentile, A. L. and O. M. Stafsudd. "Crystal Growth of $A^{II}B^{IV}C^{V}_2$ Chalcopyrites," Materials Research Bulletin 9: 105-116 (1973).

Gorban, I. S. et al. "Luminescence of Zinc Germanium Diphosphide Crystals," Sov. Phys. Semicond., 18: 892-893 (1984).

Gregg, Capt Michael R. Cathodoluminescence Spectroscopy of Zinc Germanium Phosphide. MS Thesis AFIT/GEP/ENP/92D-4. School of Engineering, Air Force Institute of Technology (AU), Wright-Patterson AFB OH, December 1992.

Hecht, Eugene. Optics. Reading, Massachusetts: Addison-Wesley Publishing Company, 1987.

Hobgood, H. M. et al. "$ZnGeP_2$ Grown by the Liquid Encapsulated Czochralski Method," Journal of Applied Physics, 73: 4030-4037 (1992).

Liboff, Richard L. Introductory Quantum Physics. San Francisco: Holden-Day Inc., 1980.

McKelvey, John P. Solid State and Semiconductor Physics. Malabar, Florida: Robert E. Krieger Publishing Company, 1966.

Miller, A. et al. "Infrared Dielectric Dispersion of $ZnGeP_2$ and $CdGeP_2$," J. Phys. Chem. Solids, 35: 685-693 (1974).

Ooe, A. et al. "Optical Studies on Off-Stoichiometry and Zn-Doping for $CuGaS_2$ Crystals." Proceedings of the7th International Conference on Ternary and Multinary Compounds. 471-476. Pittsburgh: Materials Research Society, 1987.

Pankove, Jacques I. Optical Processes in Semiconductors. New York: Dover Publications, 1971.

Shay, J. L. and J. H. Wernick. Ternary Chalcopyrite Semiconductors: Growth, Electronic Properties, and Applications. New York: Pergamon Press, 1975.

Shileika, A. "Energy Band Structure and Modulation Spectra of $A^2C^4C^5_2$ Semiconductors," Surface Science, 37: 730-747 (1973).

Sze, S. M. Physics of Semiconductor Devices. New York: John Wiley & Sons, 1981.

Vodopyanov, K. L. et al. "High Efficiency Middle IR Parametric Superradiance in $ZnGeP_2$ and GaSe Crystals Pumped by an Erbium Laser," Optics Communications, 83: 322-326 (1991).

Xing, G. C. et al. "Organometallic Chemical Vapor Deposition of Epitaxial $ZnGeP_2$ Films on (001) GaP Substrates," Journal of Crystal Growth, 94: 381-386 (1989).

Vita

Captain Jack E. McCrae, Jr. was born on 10 October 1961 in Summit, New Jersey. He graduated from Middletown High School South in Middletown, New Jersey in 1980. He graduated from the Massachusetts Institute of Technology in 1984 with a Bachelor of Science in Physics in June, 1984, obtaining a commission in the Air Force, through R.O.T.C. at the same time. He worked at the Air Force Weapons Laboratory, in Albuquerque, NM, from 1984 through 1989 as a Semiconductor Laser Development Project Officer, and at the Ballistic Missile Organization, in San Bernardino, CA, as the Small ICBM Ordnance Firing System Project Manager from 1989 through 1992. He entered the School of Engineering at the Air Force Institute of Technology in June 1992.

Permanent Address: 49 Orchard Rd
South Burlington VT
05401

REPORT DOCUMENTATION PAGE

Form Approved
OMB No. 0704-0188

1. AGENCY USE ONLY (Leave blank)	2. REPORT DATE	3. REPORT TYPE AND DATES COVERED
	13 Sep 93	Thesis

4. TITLE AND SUBTITLE

Photoluminescence Spectroscopy Of Zinc Germanium Diphosphide ($ZnGeP_2$)

5. FUNDING NUMBERS

6. AUTHOR(S)

Jack E. McCrae, Jr., Captain, USAF

7. PERFORMING ORGANIZATION NAME(S) AND ADDRESS(ES)

Air Force Institute of Technology
Engineering Physics Department
WPAFB, OH 45433-6583

8. PERFORMING ORGANIZATION REPORT NUMBER

AFIT/GAP/ENP/93S-01

9. SPONSORING / MONITORING AGENCY NAME(S) AND ADDRESS(ES)

DR MEL OHMER
WL/MLPO
WRIGHT-PATTERSON AFB OH 45433

10. SPONSORING / MONITORING AGENCY REPORT NUMBER

11. SUPPLEMENTARY NOTES

12a. DISTRIBUTION / AVAILABILITY STATEMENT

Distribution unlimited; Approved for public release

12b. DISTRIBUTION CODE

13. ABSTRACT (Maximum 200 words)

Zinc germanium diphosphide ($ZnGeP_2$) is a chalcopyrite semiconductor with strong nonlinear optical properties and potential application to Air Force interests. The characteristics of this material have been studied using photoluminescence (PL) spectroscopy. The PL spectrum is dominated by transitions from the conduction band to a deep acceptor level, and features in the spectrum suggest that more than one transition is being observed. The PL is partially polarized, and the degree of polarization appears to differ for each feature in the spectrum. The relative PL intensity of these features are seen to depend upon the wavelength of the excitation source in a fashion which suggests that the observed transitions may originate from three separate conduction bands. These experimentally observed results are found to agree qualitatively with the published band structure of $ZnGeP_2$.

14. SUBJECT TERMS

Zinc Germanium Diphosphide, Photoluminescence, Cathodoluminescence, Semiconductors, Non Linear Optics

15. NUMBER OF PAGES
61

16. PRICE CODE

17. SECURITY CLASSIFICATION OF REPORT	18. SECURITY CLASSIFICATION OF THIS PAGE	19. SECURITY CLASSIFICATION OF ABSTRACT	20. LIMITATION OF ABSTRACT
UNCLASSIFIED	UNCLASSIFIED	UNCLASSIFIED	UL